

https://dspace.org/

Modelling of gas recovery from South African shale reservoirs

Qwabe, Thembinkosi Sabelo

2019-09-09

https://hdl.handle.net/10539/29351

Qwabe, Thembinkosi Sabelo. (2019). Modelling of gas recovery from south African shale resevoirs. University of the Witwatersrand, https://hdl.handle.net/10539/29351

Downloaded from a DSpace repository. https://dspace.org/

Modelling of Gas Recovery from South African Shale Reservoirs

Prepared by

Thembinkosi Sabelo Qwabe, 857925

A Research Report submitted to

The School of Chemical and Metallurgical Engineering, Faculty of Engineering and the Built Environment, University of the Witwatersrand, Johannesburg, South Africa, in partial fulfilment of the requirements for the Degree of Master of Science in Petroleum Engineering.

Supervisor: Dr. Diakanua Nkazi

September 2019

i) Plagiarism declaration

This section serves to confirm that the work presented herein is the product of the author(s).

Any work that has been adopted from other sources has been referenced.

No work from other sources has been presented without acknowledgement.

No one has been allowed to copy the work presented in this document.

Signature: _____ Date: 09 September 2019

Abstract

Mathematical models for a triple-porosity continuum describing the distribution of pressure-the driving force for gas flow during gas production-were developed on the basis of the continuity equation from first principles, focusing on the South African shales of the Karoo Basin. The triple-porosity continuum incorporated the matrix, the natural fracture network, and the hydraulic fracture network; the matrix and the natural fracture network systems were considered two dimensional, while the hydraulic fracture system was considered one dimensional. The three developed mathematical models are in the form of the general diffusion or heat equation, thus the numerical Finite difference method (FDM) was employed in solving the triple-porosity model. MATLAB software was used to develop and solve the FDM simulation or algorithm of each system of the triple-porosity model; results for each system are presented and discussed in chapter 6 of the research report. The results generated agree with models previously developed and validated with their respective field data, substantiating the reliability of the model developed in this research report. Currently the South Africa's Barnett shale does not have field data, hence the field data from literature was used to validate the developed model. The model is thus a guide onto describing the gas flow behaviour for the South African shale gas reservoirs, and not specifically for the Barnett shale.

Table of Contents

i) Plagiarism declaration i
Abstract ii
List of Figures iv
List of Tables v
Acknowledgments vi
Chapter 1: Introduction 1
1.1 South African shale gas 1
1.2 Technologies involved in developing gas shale 2
1.2.1 Horizontal drilling 2
1.2.2 Hydraulic fracturing 2
1.3 Aim and Objectives of the research 4
1.3.1 Aim of the research 4
1.3.2 Research objectives 4
Chapter 2: Literature review 5
2.1 Dual-porosity model 5
2.2 Triple-porosity model 7
2.3 Petro-physical and thermophysical properties of the South African gas shale 9
Chapter 4: Development of the mathematical flow model 17
4.1 Model assumptions 17
4.2 Matrix phase flow model 20
4.3 Natural fracture phase 24
4.4 Hydraulic fracture phase 26
Chapter 5: Solution to the models developed 28
5.1 Hydraulic fracture phase 28
5.2 Natural fracture phase 29
5.3 Matrix phase 30
Chapter 6: Analysis of the results 32
6.1 Hydraulic fracture network 32
6.2 Natural fracture network and the matrix phase 36
Chapter 7: Conclusions and future work 42
Nomenclature 43
References 44
Appendix A: Developed triple-porosity model algorithm, simulated using MATLAB. 46

List of Figures

Figure 1. 1: Hydraulic fracturing process for extracting shale gas 3

Figure 2. 1: Idealized heterogeneous dual-porosity medium. 6
Figure 2. 2: A conceptualized triple-porosity model for gas shale at various pore distribution scale.. . 9

Figure 3. 1: A three dimensional (3D) representation of a single-cell rock formation. 13

Figure 4. 1: Schematics (a) and (b) representing the controlled volume of mass flux or flow. 18
Figure 4. 2: Schematic diagram representing the proposed physical triple porosity model. 20

Figure 6. 1: Pressure distribution with respect to time and location of the gas in the hydraulic fracture phase, where the known constant c is 2.5 33
Figure 6. 2: Pressure distribution with respect to time and location of the gas in the hydraulic fracture phase, where the known constant c is 5 34
Figure 6. 3: Pressure distribution with respect to time and location of the gas in the hydraulic fracture phase, where the known constant c is 10 35
Figure 6. 4: Pressure distribution in the natural fracture with respect to gas flow at different increasing time steps shown by (a), (b) and (c), respectively. 38

List of Tables

Table 2. 1: Petro-physical and thermophysical properties of the Ripon Formation in the Southern Karoo Basin. 10

Table 2. 2: Reservoir and horizontal well basic parameters incorporated in the simulation model.... 11

Acknowledgments

This research report is written as the final research report in the fulfilment of my Master of Science degree in petroleum engineering, a one year programme by course work and research at the University of The Witwatersrand, Johannesburg, with coursework successfully completed.

In this regard I would like to give thanks to the Lord Jesus, the invisible God for being with me from the beginning, giving me all the strength and faith to endure to this far.

I would like to pass special many thanks to my supervisor Dr. Diakanua Nkazi for believing in me and giving me the opportunity to work with him on this project, patiently guiding and supporting me in each and every milestone of the project; I am grateful.

I would like to thank my Mom for her everlasting care & support which kept me strong and enduring in this research project. I would also like to pass my thanks to my engineering colleague Nkululeko Shongwe for his suggestions and contributing to the success of the research project.

Last but not least, I would like to thank and express my gratitude to the University of The Witwatersrand, Johannesburg, for its funds and all its very helpful resources allocated for me to make this research project and my academics a success.

Chapter 1: Introduction

1.1 South African shale gas

Shale gas being the cleanest fossil fuel now produced in large amounts in developed countries such as the United States of America, and also it being anticipated as the future leading energy source, it has recently been discovered also in South Africa, trapped in shales of the Karoo Basin of the Eastern and the Western Cape Provinces (Geel, Schulz, Booth, & deWit, 2013).

Under the investigation of the lower Ecca Group of the Karoo Supergroup by (Geel, Schulz, Booth, & deWit, 2013), the Southern Karoo Basin was discovered to cover an estimated area of 300 000 square kilometres, and it was predicted to have a potential reserve of between 32 to 485 trillion cubic feet (Tcf), of most conservative prediction is gas resource. The Ecca Group is a group of sedimentary formations mostly composed of fine-grained graywacke, sandstone, bluish-black shale (Ryan, 1978). One of the famous Ecca Group are the Prince Albert Formation, which is composed of mudstone with shale, and some sandstone units, and the Whitehill Formation which is composed of fine-grained, black organic rich shale; these formations date back as early as 100 million years ago (Geel, Schulz, Booth, & deWit, 2013). On the investigation conducted by (Geel, Schulz, Booth, & deWit, 2013) on the lower Ecca Group of the Eastern Cape, the Whitehill Formation was concluded to have a total organic carbon (TOC) content which qualifies it as a successful gas-bearing shale, with an average TOC content of 4.5% by weight; 0.5% TOC is considered the minimum value by weight for a formation to be considered an effective source rock. Therefore, the Whitehill Formation is the focusing point for potential shale gas exploration and development in the Southern Karoo (Geel, Schulz, Booth, & deWit, 2013).

The increase in global energy demand has led to a drastic decline on the conventional oil & gas (fossil fuels) reserves; this has compelled the oil & gas industries to look for alternative ways of exploiting these fossils in order to sustain the energy in demand, for over many generations (Wang, Torres, Xiang, Fei, & Naido, 2015).

Unconventional reservoirs, well-known as shale in the reservoir engineering perspective, so far are the most focused-on alternative sources of oil & gas, mainly for accessing natural gas. Petroleum/oil & gas reservoirs, which are defined as subsurface pool of hydrocarbons, are known to be contained in porous rock formations with many cracks, or simply fractures in the

geology point of view. The American Association of Petroleum Geologists (AAPG) defines a fractured reservoir as a reservoir with which its naturally occurring fractures have a significant effect on the reservoir fluid flow; this effect the natural fractures have on the reservoir fluid flow is predicted to be in a form of increased reservoir permeability, porosity, and/or increased permeability anisotropy (Nelson, 2001); these are the most important parameters that will be looked at and applied in developing the mathematical model forecasting the recovery or production of shale gas in terms of flow, particularly in South Africa.

1.2 Technologies involved in developing gas shale

There are two technologies applied in exploiting oil & gas from unconventional reservoirs, namely: Horizontal drilling, and hydraulic fracturing (Industry, 2017).

1.2.1 Horizontal drilling

Horizontal drilling is a process of drilling a well from the surface, vertically downwards to the subsurface of a sea, just above the targeted oil or gas reservoir (Industry, 2017). The drilled well is then oriented into a horizontal direction to enhance contact with the oil or gas in place. This process is mainly applied for gas field (shale) development, while in the development of conventional oil & gas reservoirs the well is only drilled vertically; see figure. 1.1 as an example on the orientation during horizontal drilling.

1.2.2 Hydraulic fracturing

After horizontal drilling has been completed, hydraulic fracturing process, or simply fracking follows; this process takes place in stages, starting at the end of a wellbore after the horizontal section of the well has been drilled. Hydraulic fracturing is a process of creating a complex network of cracks in the shale formation by pumping a fracturing fluid through the wellbore under high pressure; a fracturing fluid is usually composed of water, sand or organic clay, and a variety of additives depending on the petrophysics of the formation (Montgomery, 2013). Figure 1.1 below depicts a diagram briefly outlining the hydraulic fracturing process.

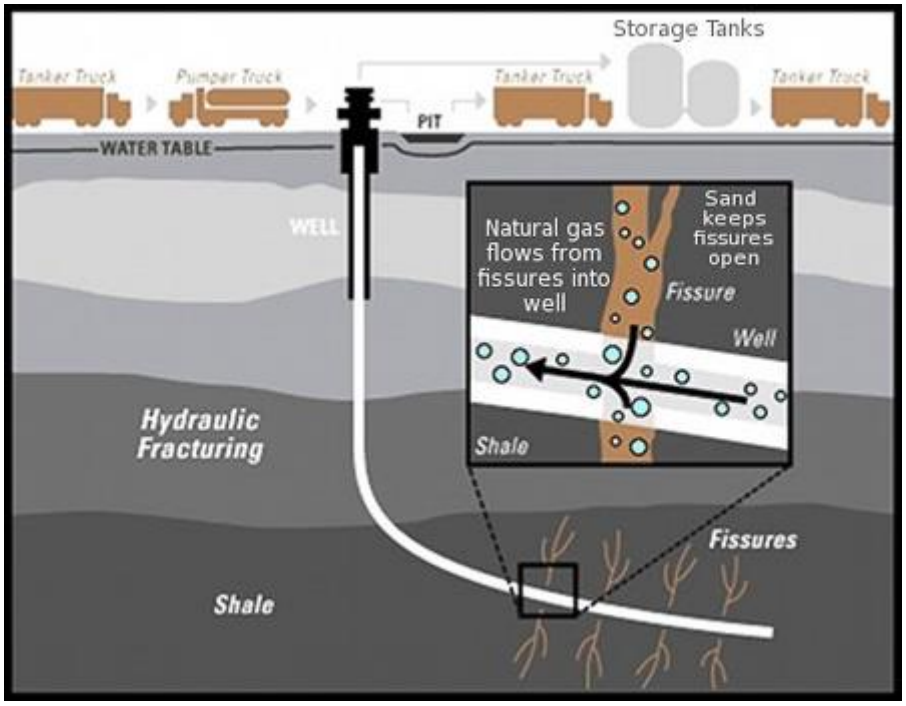


Figure 1. 1: Hydraulic fracturing process for extracting shale gas (Scally, 2012).

The sand of the pressurized fracturing fluid opens the shale, thus creating a pathway for the oil or gas to flow up the well; this technology was adopted in the oil & gas industry as early as in the 1940s, recovering more than 600 trillion cubic feet of natural gas and 7 billion barrels of oil (Industry, 2017). This process is carried out in several stages, summarised in steps listed below:

Step 1 – A perforating gun in a casing inside the drilled hole (wellbore) is placed into the targeted position, where an electric current is used to shoot tiny holes through the casing into a shale formation; this is where the fracturing fluid opens a pathway for shale gas to flow from the formation into the wellbore. Formation perforation and fracturing are performed in several cycles, preparing for production section by section; cycles are presented in a video from (Chevron, 2014).

Step 2 – Repeat in stages: During each fracking stage, the process parameters (i.e. fracking pressure) are monitored, adjusted and recorded to ensure safe work environment.

Step 3 – After each stage is completed, a plug is pumped down the casing to isolate stages as new perforations are created to direct the fracturing fluid to the next stage; the segmentation of the well in stages or section by section allows the shale gas to be produced in greater amounts from the lateral length of the well.

Step 4 – After hydraulic fracturing has been completed, all the plugs pumped down the casing are drilled out of the completed well, safely removing the fracturing fluid from the formation so that shale gas can be extracted. The removed fracturing fluid from each well is treated and reused.

Step 5 – The sand of the fracturing fluid remains in the shale, keeping the gas pathway open as the gas flows into the wellbore, and then to the surface where it is processed.

Three different porous media with different porosities and rock permeability are involved in gas shale development, which means different capacities for storing gas and conducting its flow respectively; and because of their very low porosity and permeability the gas is stimulated by the application of the two above outlined technologies involved in developing shale gas resources, unlike conventional reservoirs whose porosity and permeability are higher and thus are only drilled vertically as they require minimal stimulation. This is the motivation behind developing a triple continuum flow model for unconventional reservoirs.

1.3 Aim and Objectives of the research

1.3.1 Aim of the research

The aim of the research is to develop a mathematical flow model derived from first principles, for the South African shale gas, incorporating the different porous media, focusing on the KWV-1 bore hole drilled in the Eastern Cape province of South Africa in 2015.

1.3.2 Research objectives

- To establish the triple porosity model for the general shale gas reservoir using the petrophysical and thermophysical properties data of the South African shale reservoir (from the KWV-1 borehole), that is currently available from literature.
- To develop mathematical flow models of the different porous media considering a triple porosity continuum.
- To investigate the effect of permeability of hydraulic fractures on the production rate.
- To investigate the effect of the initial pressure ($p_m = p_{NF} = p_{HF} = p_i$) on the production rate.
- To validate the model by using field data and simulation from literature.

Chapter 2: Literature review

2.1 Dual-porosity model

The flow of reservoir fluids to the wellbore begins from the fractures system, followed by a transition period where the fluids begin to flow from the matrix to the fractures. Finally, equilibrium is reached where the fluids now flow from the matrix to the fractures, and then to the producing wellbore (Ezekwe, 2011). Porosity of a shale reservoir defines the capacity of the reservoir matrix and/or fractures system to store reservoir fluids, while permeability on the other hand measures the capacity of the reservoir matrix and/or fractures system to transport the reservoir fluids (Ezekwe, 2011); these are the most important parameters in developing a model forecasting the production of shale gas (Wang, Torres, Xiang, Fei, & Naido, 2015).

Shale gas, a very important source of natural gas, is one of the reservoir fluids contained in large quantities in fractured reservoirs (Alahmadi, 2010). Petroleum reservoir fluids are normally stored in the matrix and natural fractures, and the total system is named the double porosity/permeability model, or dual-porosity model (Ezekwe, 2011). Researchers have developed and applied different conceptual models to model dual-porosity interaction; among the common methods, they used: (a) explicit discrete-fracture and matrix model, (b) dual-continuum model, and (c) effective-continuum model (Mohammadi & Manshad, 2012). Dual-porosity models are traditionally used to model naturally fractured reservoirs, which have two distinct porosities-the matrix porosity and the natural fractures porosity for storing reservoir fluids; figure. 2.1 below depicts one of the popular idealized heterogeneous dual-porosity model (medium/or reservoir), by (Warren, 1963).

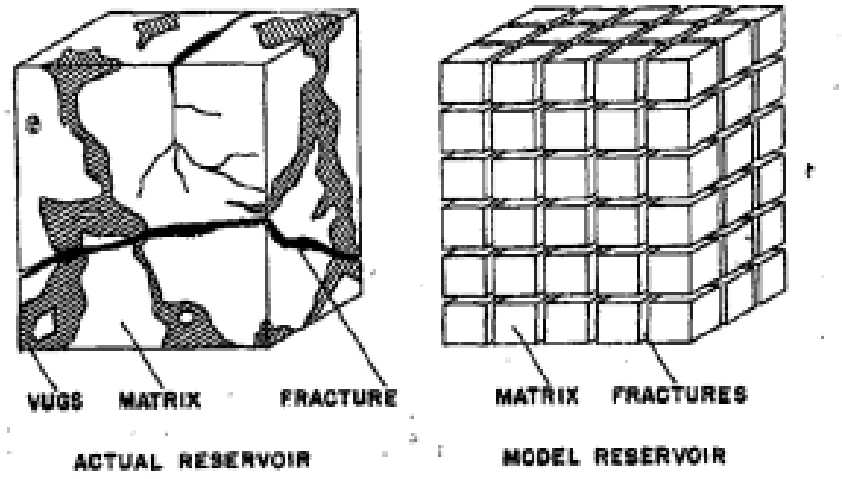


Figure 2. 1: Idealized heterogeneous dual-porosity medium (Warren, 1963).

Dual-porosity models are categorized into two categories according to their flow conditions: pseudo-steady state flow models and unsteady state flow models, under the interporosity fluid transfer assumption (Alahmadi, 2010).

Pseudo-steady state interporosity flow model

Many naturally fractured reservoirs exhibit this type of flow model, which describes the flow of fluids from the matrix to the fractures to be occurring instantaneously (Ezekwe, 2011). The flow is defined by the equation (1) shown below, which holds for any dual-porosity/dual-permeability simulator (Rangel-German, 2003).

$$q = \alpha \frac{k*V}{\mu}(p_m - p_f) \qquad (1)$$

q is the flow rate in a reservoir of bulk volume V, p_m is the volumetric average matrix pressure, and p_f is the fracture-pressure. The α parameter is the shape factor reflecting the matrix geometry, where the system is pseudo-steady state, single-phase flow at all times (Rangel-German, 2003).

Many years back, (Warren, 1963) proposed the pseudo-steady state model to describe the flow in the dual-porosity interaction, however due to several drawbacks and it being an analytical approach, numerical approaches have been proposed to modify the Warren's model, and these numerical approaches have been reported to have improved the results obtained by an analytical solution (Mohammadi & Manshad, 2012).

Unsteady state interporosity flow model

In this interporosity flow model the flow is unsteady (or transient) between the matrix and fractures, and the model produces similar results as the pseudo-steady state interporosity flow model, except for the transition period between the matrix and fractures (Alahmadi, 2010). Interporosity fluid transfer describes the mass transfer of reservoir fluids between the matrix and the fractures system; its measure is called the interporosity flow coefficient (Ezekwe, 2011).

2.2 Triple-porosity model

(Wang, Reed, & John, 2009) investigated potential effects of organic matter on petro-physical properties, pore networks, and on the fluid flow in gas shales using pore images and geochemical data of the Barnett Shale; after their investigation, they found that there are four types of porous media in gas shale systems: nonorganic matter, organic matter/kerogen, natural fractures, and hydraulic fractures. According to their investigation, organic matter, which has pores ranging from 5 to 1000 nm is especially important amongst the mentioned porous media; this is because the pores of the organic matter adsorbing and storing free natural gas or methane are much higher than the pores of nonorganic matrix. The nonorganic matrix is therefore considered negligible (Wei, Liu, & Elsworth, 2018). Pore spaces are thought to be organic when oil and/or gas molecules are generated in them (Wang, Reed, & John, 2009). In order to describe the complexity of gas shale systems, a triple-porosity model is the proposed approach, improving on the dual-porosity model, where only the matrix and natural fractures are considered (Wei, Liu, & Elsworth, 2018).

(Wei, Liu, & Elsworth, 2018) researched and found several authors who have developed triple-porosity models, one author or authors building from another author's work, and each assuming different flow mechanisms; however they also found that all the authors' models neglected the geomechanical effects on the gas flow, which are important in determining shale permeability, and cannot be ignored in modelling gas recovery (Wang, Luo, Liu, Lin, & Li, 2016). They established their triple-porosity model comprising the kerogen matrix system, inorganic matrix system, and natural fractures system, and it was valid over the whole range of flow regimes in shale. Their model combined the multiscale flow incorporating the geomechanical effects.

A triple-porosity model is a model comprising three porous media; they are kerogen (organic matrix), the nonorganic matrix, and the fractures system-either natural fractures or hydraulic fracture system. With kerogen or organic matrix having a massive storage for adsorbed gas in gas shale, and the nonorganic matrix considered negligible of gas, a triporosity model comprising of the organic matrix, the natural fractures-where free gas is also stored (Wei, Liu, & Elsworth, 2018), and the hydraulic fractures will be assumed in conducting this research; this assumption establishes the triple porosity model, which is the first objective of the research.

However, it is also known that most kerogen or the organic matrix is disorderly distributed within the nonorganic matrix, and since kerogen is the matrix where gas transfer is channelled from, means that any other porous medium or system in the shale will communicate with kerogen through a few nano-pores of the nonorganic matrix (Wei, Liu, & Elsworth, 2018). (Wei, Liu, & Elsworth, 2018) proposed their triporosity system based on a multispace scale of pore distribution; figure 2.2 below shows their conceptualized triporosity model for gas shale at various pore distribution scale.

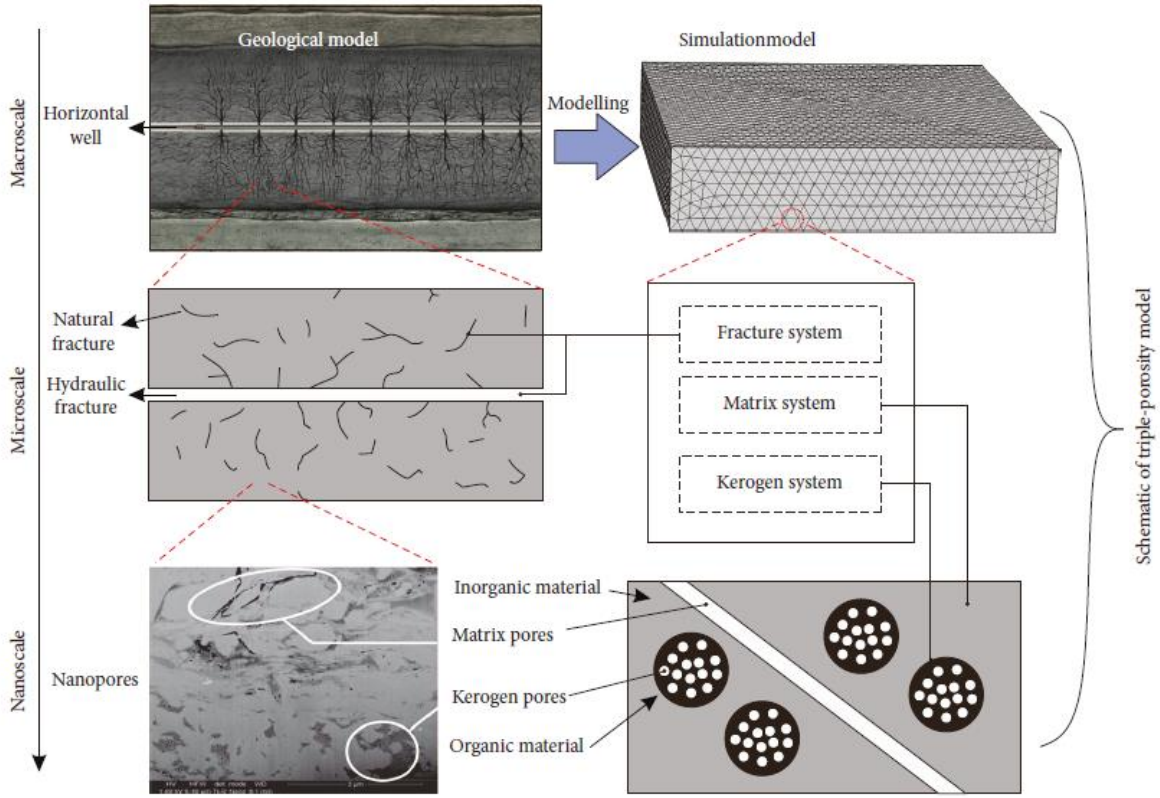


Figure 2. 2: A conceptualized triple-porosity model for gas shale at various pore distribution scale (Wei, Liu, & Elsworth, 2018).

They concluded that the matrix system is the main source of free gas, while the natural fractures' permeability mainly contributes in measuring the capacity to transport gas. They also reported that the rate of production of shale gas is strongly dependent on the hydraulic fractures, which are a highway for gas transfer from the shale matrix surrounded by natural fractures, to the horizontal well. This is simply because hydraulic fractures have a higher permeability (Alahmadi, 2010).

2.3 Petro-physical and thermophysical properties of the South African gas shale

(Campbell & Mielke, 2016) studied the first deep Karoo borehole, a KWV-1 borehole in the Eastern Cape Province of South Africa, and their studied drilled core is curated at one of the National Science Councils of South Africa-the Council for Geoscience (GCS) in Pretoria.

They reported that the borehole intersects six formations of the Ecca Group sedimentary formations, as well as of the Beaufort and the Dwyka Groups-other group of sedimentary formations discovered in South Africa.

In conducting their experiment they selected 32 core samples across the Ripon formation members, which are also intersected in the borehole KWV-1; the lithology of these samples ranges from siltstone to medium-grained and very fine-grained, partly organic-rich sandstone (Campbell & Mielke, 2016). Petro-physical and thermophysical properties of the 32 selected samples were measured and analysed at the TU Darmstadt's geothermal laboratory. Below is a table of results of the petro-physical and thermophysical properties from KWV-1 borehole, obtained by (Campbell & Mielke, 2016).

Table 2. 1: Petro-physical and thermophysical properties of the Ripon Formation in the Southern Karoo Basin (Campbell & Mielke, 2016).

Sample location	**KWV-1 (Borehole)**
Number of measurements	32
Density (kg/m^3)	2570-2770
Mean density (kg/m^3)	2700
Porosity (%)	0.40-2.20
Mean porosity	1.3
Permeability (mD)	0.0010-0.0020
Mean permeability (mD)	0.0014
Thermal conductivity (W/m.K)	3.17-3.71
Mean thermal conductivity (W/m.K)	3.37
Thermal diffusivity ($1x10^{-6}$ m^2/s)	1.30-1.53
Mean thermal diffusivity ($1x10^{-6}$ m^2/s)	1.39

In conducting this research, these petro-physical and thermophysical properties will be used in modelling gas recovery from South African shale reservoirs (KWV-1 borehole). Additionally to the above data, data from (Jiang & Xu, 2017) and (Guo & Wei, 2015), shown in Table 2.2 below will also be incorporated in this research.

Table 2. 2: Reservoir and horizontal well basic parameters incorporated in the simulation model (Jiang & Xu, 2017), (Guo & Wei, 2015).

Parameter	Symbol	Units	Value
Reservoir length,		m	1300
Reservoir breadth		m	600
Effective thickness		m	20
Fracture half-length		m	146
Fracture spacing	r_e	m	100
Wellbore radius	r_w	m	0.1
Initial reservoir pressure	p_i	MPa	20
Bottom-hole pressure	p_w	MPa	5
Initial reservoir temperature	T	K	350
Langmuir pressure	p_L	MPa	5
Langmuir volume	V_L	m^3/kg	2.83×10^{-3}
Porosity of the matrix phase	ϕ_m	dimensionless	0.05
Porosity of the natural fracture	ϕ_{NF}	dimensionless	0.01
Porosity of the hydraulic fracture	ϕ_{HF}	dimensionless	1
Natural fracture permeability	k_{NF}	mD	0.05
Hydraulic fracture permeability	k_{HF}	mD	8000
mf interface area per rock volume	A_{mNF}	m^{-1}	50
fF interface area per rock volume	$A_{NF\rightarrow HF}$	m^{-1}	0.5
NF characteristic length	L_{NF}	m	0.1
HF characteristic length	L_{HF}	m	1
Gas viscosity	μ_g	Pa.s	1.02×10^{-5}
Gas standard molar volume	V_{std}	m3/kmol	22.4
Gas molecular weight	M	kg/kmol	16

Chapter 3: Adsorption/Desorption in Shale Gas Reservoirs

The production of shale gas is reported to take place by desorption and diffusion of gas in the pore spaces of the matrix, and then flows into fractures by Darcy flow (Berawala, 2015). During production, the free gas stored in the natural fractures is produced first, and thereafter the adsorbed gas within the kerogen/or organic and nonorganic matrix feeds the fracture system. However, the nonorganic matter has much bigger pores classified as micro-fractures relative to the organic matter, and it only starts producing after the formation has been hydraulically fractured, thus it is agreeable to define the organic matter as the matrix, while the nonorganic matter is defined as micro-fractures (Berawala, 2015). This means that gas is only adsorbed on the organic/or kerogen matrix surface, for ease of modelling. Desorption of gas from the organic matrix takes place when the pressure inside the matrix declines during production; this desorbed gas acts as free gas within the matrix, and then as a source of gas feeding to the micro-fractures system (Berawala, 2015). The flow of gas in this system can either be Darcy or non-Darcy flow, depending on the rate at which the gas is channelled and the Reynold's number of the gas.

Figure 3.1 below shows a simplified/or single-cell model of the shale rock formation used in FORTRAN code for shale gas production (FSGP). When the cells are put together they form a reservoir linked to a producing well, such that the gas flow is from one cell to another, then to the well through hydraulic fractures (Berawala, 2015). This is the sequence of flow of gas; no gas flows from the matrix directly to the well, and of course there are assumptions involved.

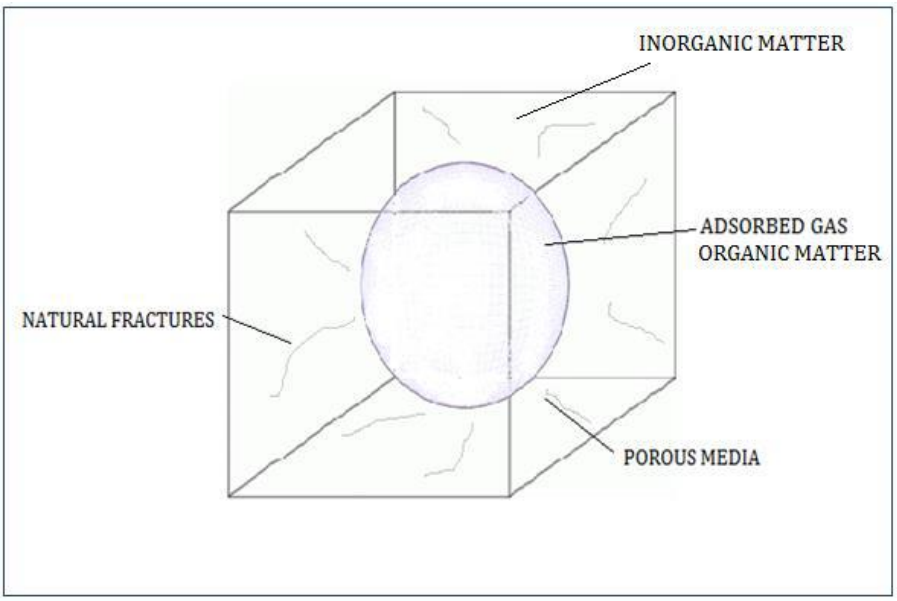


Figure 3. 1: A three-dimensional (3D) representation of a single-cell rock formation (Berawala, 2015).

The sphere can be viewed as a group of layers of the adsorbed gas. Gas desorption begins at the outermost layer of the sphere (kerogen/or organic matter) when the pressure lowers to the critical desorption pressure as the pressure declines in the matrix; this desorbed gas diffuses out of kerogen, and then desorbs into the micro-fractures (inorganic matter) represented as the box of the cell, until all the gas layers diffuse out of the kerogen. The total gas content adsorbed in the organic matter (sphere) is given by Langmuir's Isotherm (Berawala, 2015), given as below:

$$V_{ads} = V_L * \frac{p}{P + P_L} \qquad (2)$$

where V_{ads} = gas content in volume of gas per unit mass of shale matrix (m^3/kg),

V_L = Langmuir's volume, the maximum amount (standard volume) of adsorbed gas at infinite pressure in a shale matrix (m^3/kg),

p = the reservoir pressure (Pa), and

p_L = Langmuir's pressure (or critical desorption pressure), the pressure at which one-half of the Langmuir's volume can be adsorbed (Pa).

(Berawala, 2015) who also studied about the modelling of shale gas, found that the approximated values of V_L and P_L are 218.57 scf/ton and 2695.57 psi, respectively for the Barnett shale. Kerogen or organic matter is the most important factor when determining the

gas content adsorbed on to shale as it affects the size and structure of pores in the matrix-which determine the surface area available for adsorption; the features of organic matter include the type of organic matter, the total organic carbon (TOC) content, and thermal maturity of the shale formation (Berawala, 2015). V_L is a function of TOC and the thermal maturity of shale.

Adsorption of shale gas on the surface of nanopores follows the mono-layer Langmuir isotherm equation (Yao, Wang, & Sun, 2015):

$$q_{ads} = \frac{\rho_s . M_g}{V_{std}} . V_{ads} \qquad (3)$$

where q_{ads} = Mass of adsorbed gas per unit volume of shale matrix, kg/m^3

ρ_s = Shale matrix (sphere) bulk density, kg/m^3

M_g = Molecular weight of shale gas at standard temperature and pressure, kg/kmol

V_{std} = Molar volume of shale gas at standard conditions, m^3/kmol

Substituting Langmuir's isotherm volume into equation (3) gives:

$$q_{ads} = (\frac{\rho_s . M_g}{V_{std}}) . V_L * \frac{p}{\mathrm{P} + \mathrm{PL}}$$

Differentiating this equation with respect to time gives the mass flow rate of adsorbed gas per volume of shale matrix:

$$\frac{\partial q_{ads}}{\partial t} = \frac{\partial}{\partial t}\left(\left(\frac{\rho_s . M_g}{V_{std}}\right) . V_L * \frac{p}{\mathrm{P} + \mathrm{PL}} \right)$$

$$\frac{\partial q_{ads}}{\partial t} = \frac{\rho_s . M_g}{V_{std}} . V_L * \frac{\partial}{\partial t}\left(\frac{p}{\mathrm{P} + \mathrm{PL}}\right)$$

V_L, ρ_s, M_g, and V_{std} are constants and thus can be factored out; differentiating the $\frac{\partial}{\partial t}(\frac{p}{\mathrm{P+PL}})$ part by applying the quotient rule gives:

$$\frac{\frac{\partial p}{\partial t}(\mathrm{P} + \mathrm{PL}) - \frac{\partial(\mathrm{P} + \mathrm{PL})}{\partial \mathrm{t}} p}{(\mathrm{P} + \mathrm{PL})^2}$$

which, after simplification (noting that PL is also a constant), gives:

$$\frac{\partial p}{\partial t} * \frac{1}{(\mathrm{P} + \mathrm{PL})^2} * \mathrm{PL}$$

Therefore the whole equation describing adsorption rate per shale matrix volume is then given by equation (4):

$$\frac{\partial q_{ads}}{\partial t} = \frac{\rho_s . M_g}{V_{std}} * V_L * \mathrm{PL} * \frac{1}{(\mathrm{P}+\mathrm{PL})^2} \frac{\partial \mathrm{p}}{\partial \mathrm{t}} \qquad (4)$$

where $\frac{\partial q_{ads}}{\partial t}$ = Mass flowrate of adsorbed gas per unit volume of shale matrix, kg/m^3.s

The rate of desorption of gas has a significant effect on the production of gas as it maintains the reservoir pressure which is the driving force for production of free gas in the fractures system; it can be expressed as:

$$-\frac{\partial q_{ads}}{\partial t} = -\frac{\rho_s . M_g}{V_{std}} * V_L * \mathrm{PL} * \frac{1}{(\mathrm{P}+\mathrm{PL})^2} \frac{\partial \mathrm{p}}{\partial \mathrm{t}} \qquad (4b)$$

Note, desorption is the reverse of adsorption, hence the negative sign.

From the above latter equation, it can be seen that desorption rate is dependent only on the matrix or reservoir pressure, i.e. desorption is a function of reservoir pressure.

Original Gas in Place (OGIP)

The original gas in place (OGIP) in gas shales is defined as the sum of the free gas stored in pores and fractures, the gas adsorbed onto organic and inorganic matter, and the gas dissolved in oil and/or water; in this research the gas dissolved in oil and/or water is not considered, therefore the total gas in shale is the sum of free stored gas and the adsorbed gas onto organic matter only. Free gas stored in pores and fractures is considered to be in the region between the cube (micro-pores/or inorganic matter) and the sphere (Kerogen/or organic matter); the size of the sphere represents the total amount of gas adsorbed on kerogen.

The general formula for determining the OGIP, along with the necessary geological and petrophysical data, is given below:

$$G = \frac{Ah\emptyset S_{gi}}{B_{gi}}$$

where A*h = Drainage rock volume where gas is present,

Ø = Porosity, rock volume fraction available to store fluids,

S_{gi} = Saturation of gas component i, and

B_{gi} = Gas formation volume factor

Taking the following assumptions:

- Gas desorption is dependent on the reservoir pressure only, defined by the Langmuir's isotherm.
- Free stored gas and the gas desorbed reach equilibrium immediately, and are ideally mixed once the reservoir pressure attains to critical desorption pressure (Langmuir's pressure).
- Single phase flow of gas in a two-dimensional (2D) reservoir is considered; i.e. amount of water in the reservoir is insignificant, thus it's a dry-gas reservoir.

The OGIP used to estimate hydrocarbons (gas in this case) can be given as:

$$G = \frac{V_c \emptyset S_g}{B_g} + (V_L . \frac{p_i}{p_L + p_i}) * \rho_s * V_b$$

where V_c = Volume of matrix (cube),

S_g = Volume porosity filled with gas (methane),

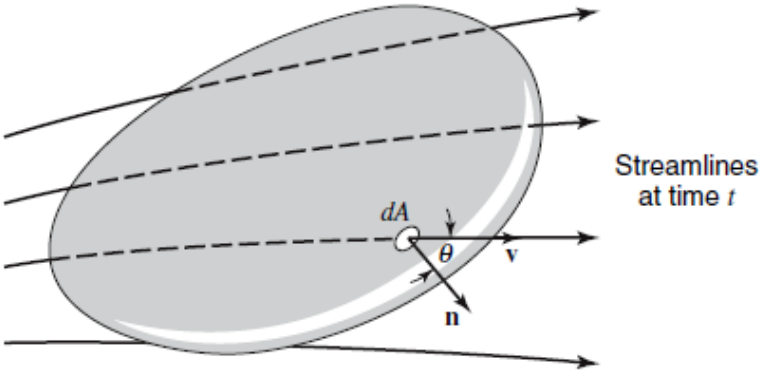
p_i = Initial reservoir pressure, and

V_b = Shale formation (sphere) bulk volume.

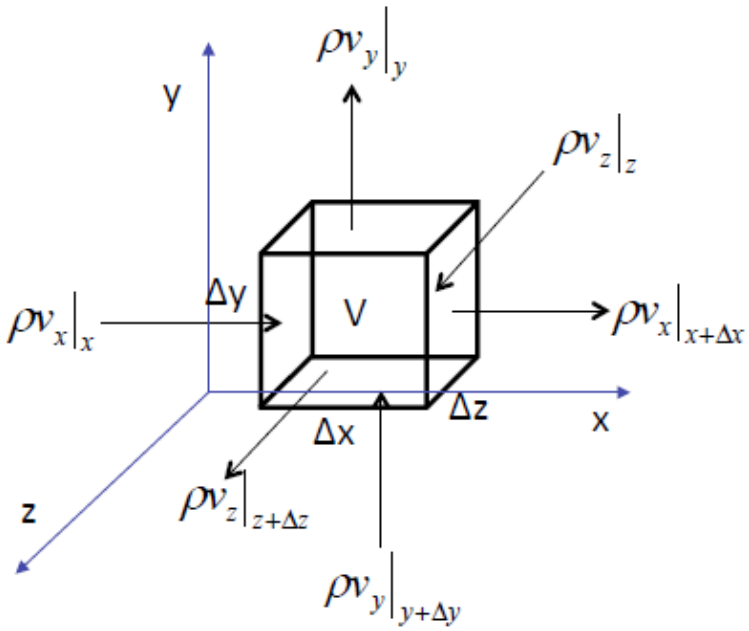
Chapter 4: Development of the mathematical flow model

4.1 Model assumptions

- The model is a triple continuum comprised of the matrix, the natural fractures, and hydraulic fractures systems; the non-organic matrix is assumed to be negligible of gas.
- The model is assumed one dimensional for the hydraulic fracture phase, and two dimensional for the matrix and the natural fracture phases.
- The flow of gas is assumed to be consecutive from the matrix to the natural fractures, then to the hydraulic fractures.
- The density of gas is assumed to be constant during flow at the control surface, however it changes in the control volume during accumulation (adsorption and/or desorption).
- The viscosity of gas is assumed to be constant; this is because only methane gas (CH_4) is considered ”gas” amongst the natural gas, in this research report.
- Gravity effects are considered negligible.
- The temperature of the reservoir is assumed to remain constant.



(a)



(b)

Figure 4. 1: Schematics (a) and (b) representing the controlled volume of mass flux or flow.

The continuity equation defining the conservation of mass will be applied as the fundamental basis for deriving the mathematical flow model for the matrix, the natural fracture, and the

hydraulic phases; the equation is defined below, starting by representing the law of conservation of mass in words:

$$\begin{pmatrix} rate\ of\ mass \\ efflux\ from \\ control\ volume \end{pmatrix} - \begin{pmatrix} rate\ of\ mass \\ flow\ into \\ control\ volume \end{pmatrix} + \begin{pmatrix} rate\ of \\ mass\ accumulation\ within \\ control\ volume \end{pmatrix} = 0$$

Considering the above general control volume, which is located in a fluid flow field (shale reservoir), the rate of mass efflux = $(\rho v)(dA\cos\theta)$, where dA cosθ is the area (dA) projection in the field normal to the velocity vector **v**, and θ is the angle between **v** and the unit vector **n** normal to dA:

$$(\rho v)(dA\cos\theta) = \rho dA\,|\boldsymbol{v}||\boldsymbol{n}|cos\theta$$

Which gives $\rho(\boldsymbol{v}.\boldsymbol{n})dA$ after recognition of the scalar or dot product from vector algebra (Welty, Wicks, & Wilson, 2008). Integrating the quantity (mass) over the whole control surface gives

$$\iint \rho(\boldsymbol{v}.\boldsymbol{n})dA$$

which is the net mass efflux from the control volume; note that the sign describing if the flow is out (efflux) or into (influx) the control volume is determined by the angle θ; i.e. 90° < θ ≤ 180° for influx (into dA), thus the sign is negative, and 0° ≤ θ < 90° for efflux (out of dA), thus the sign is positive. From Figure 4.1 above, this equation can be written as

$$(\rho v_x|_{x+\Delta x} - \rho v_x|_x)\Delta y\Delta z + \left(\rho v_y\big|_{y+\Delta y} - \rho v_y\big|_y\right)\Delta x\Delta z + (\rho v_z|_{z+\Delta z} - \rho v_z|_z)\Delta x\Delta y$$

The rate of mass accumulation within the control volume is expressed as

$$\frac{\partial}{\partial t}\iiint \rho dV$$

and from Figure. 4.1 above, it can be written as

$$\frac{\partial}{\partial t}\iiint \rho dV = \frac{\partial}{\partial t}(\rho\Delta x\Delta y\Delta z)$$

To account for porosity, knowing that gas is only stored and adsorbed in pores other than into/onto the total (bulk) volume of the matrix, the above latter equation can be written as

$$\frac{\partial}{\partial t}\iiint \rho dV = \frac{\partial}{\partial t}(\phi\rho\Delta x\Delta y\Delta z)$$

Summing the net mass efflux with the rate of mass accumulation over the entire general control volume, the continuity or Law of Conservation of mass equation becomes

$$\iint \rho(\boldsymbol{v}.\boldsymbol{n})dA + \frac{\partial}{\partial t}\iiint \rho dV = 0$$

which, after dividing by the control volume $\Delta x\Delta y\Delta z$ and taking the limit as $\Delta x\Delta y\Delta z$ approaches zero, is the same as

$$\frac{\partial}{\partial x}(\rho v_x) + \frac{\partial}{\partial y}(\rho v_y) + \frac{\partial}{\partial z}(\rho v_z) + \frac{\partial(\phi\rho)}{\partial t} = 0$$

$$\nabla.\rho\mathbf{v} + \frac{\partial(\phi\rho)}{\partial t} = 0 \qquad (5)$$

This is the continuity equation which will be used as the fundamental basis in deriving the mathematical flow model.

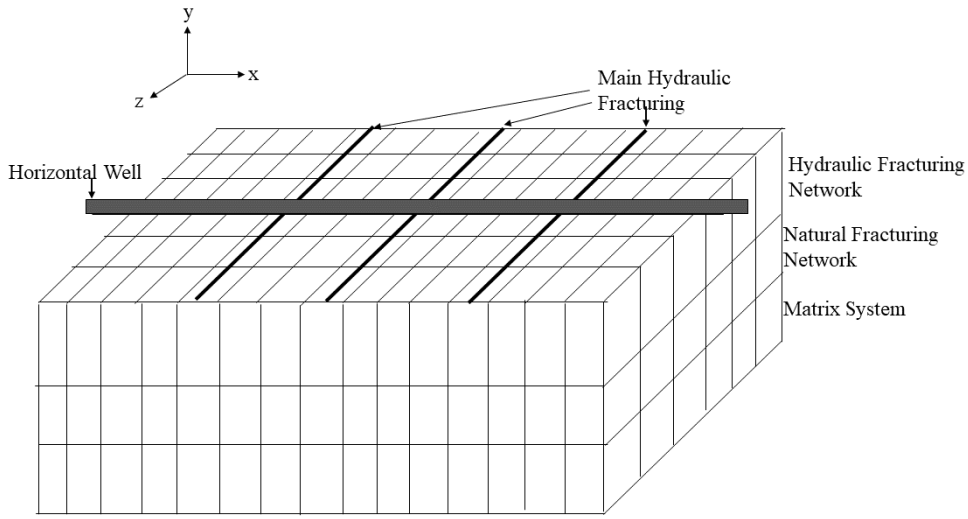


Figure 4. 2: Schematic diagram representing the proposed physical triple porosity model (Zhang, et al., 2017).

The above diagram, Figure 4.2 is the representation of the physical triple porosity model proposed in this research, and at the top corner in the left is the chosen coordinate system xyz.

4.2 Matrix phase flow model

In the matrix system (sphere) two forms of gas exist, free gas stored in the pores of the matrix, and gas adsorbed onto the kerogen/or organic matrix

$$mass\ of\ gas\ in\ the\ matrix = free\ gas + adsorbed\ gas$$

$$mass\ of\ gas\ in\ the\ matrix = \rho_g \phi_m + \rho_g V_{ads} * \rho_s \qquad (6)$$

where $\rho_g$is the gas density, which can be represented as $\rho_g = \frac{pM}{zRT}$, where M is the gas (methane) molecular weight and R = 8.314×10^3 (J/kmol.K); density is a function of temperature and pressure, thus it changes with pressure in the accumulation (adsorption or desorption) term within the control volume, and it is assumed constant on the reservoir control surface during gas flow.

Note that the subscripts *g*, *m*, *NF*, and *HF* represent gas, matrix, natural fracture, and hydraulic fracture, respectively.

The rate of mass accumulation will then be the derivative of the mass of gas in the matrix with time,

$$\frac{\partial}{\partial t}\left(\rho_g \phi_m + \rho_g V_{ads} * \rho_s\right) = \frac{\partial}{\partial t}\left(\frac{pM}{zRT}\phi_m\right) + \frac{\partial}{\partial t}\left(\rho_g V_{ads} * \rho_s\right)$$

$\frac{\partial}{\partial t}\left(\rho_g V_{ads} * \rho_s\right)$ is the rate of gas adsorption per shale matrix volume, which is

$$\frac{\partial}{\partial t}\left(\rho_g V_{ads} * \rho_s\right) = \frac{\partial q_{ads}}{\partial t} = \frac{\rho_s M}{V_{std}} * V_{L} * \mathrm{PL} * \frac{1}{(\mathrm{P} + \mathrm{PL})^2}\frac{\partial \mathrm{p}}{\partial \mathrm{t}}$$

therefore

$$\frac{\partial}{\partial t}\left(\rho_g \phi_m + \rho_g V_{ads} * \rho_s\right) = \frac{\partial}{\partial t}\left(\frac{p_m M}{zRT}\phi_m\right) + \frac{\rho_s M}{V_{std}} * V_{L} * \mathrm{PL} * \frac{1}{(p_m + \mathrm{PL})^2}\frac{\partial p_m}{\partial \mathrm{t}}$$

$$\frac{\partial}{\partial t}\left(\rho_g \phi_m + \rho_g V_{ads} * \rho_s\right) = \frac{M}{zRT}\phi_m * \frac{\partial p_m}{\partial t} + \frac{\rho_s M}{V_{std}} * V_{L} * \mathrm{PL} * \frac{1}{(p_m + \mathrm{PL})^2}\frac{\partial p_m}{\partial \mathrm{t}}$$

$$\frac{\partial}{\partial t}\left(\rho_g \phi_m + \rho_g V_{ads} * \rho_s\right) = \frac{\partial p_m}{\partial t}\left(\frac{M}{zRT}\phi_m + \frac{\rho_s M}{V_{std}} * V_{L} * \mathrm{PL} * \frac{1}{(p_m + \mathrm{PL})^2}\right) = \frac{\partial(\phi\rho)}{\partial t} \qquad (7)$$

For the net mass efflux, employing the assumption that the reservoir is two dimensional (2-D), and the coordination system

$$\nabla . \rho \mathbf{v} = \frac{\partial}{\partial x}\left(\rho_g v_x\right) + \frac{\partial}{\partial y}\left(\rho_g v_y\right) \qquad (8)$$

The velocity flow vector in the matrix can be expressed in the form of Darcy's law (Shen, Li, Xu, & Sun, 2017)

$$\boldsymbol{v} = -\frac{1}{\mu}\boldsymbol{K}.(\nabla p)$$

$$\boldsymbol{For\ x\ and\ y\ direction}\ (\boldsymbol{2-D})$$

$$v_x = -\frac{k_x}{\mu_g}\left(\frac{\partial p_m}{\partial \mathrm{x}}\right)$$

$$v_y = -\frac{k_y}{\mu_g}\left(\frac{\partial p_m}{\partial \mathrm{y}}\right)$$

Therefore

$$\nabla.\rho\mathbf{v} = \frac{\partial}{\partial x}\left(\rho_g * -\frac{k_x}{\mu_g}\left(\frac{\partial p_m}{\partial \mathrm{x}}\right)\right) + \frac{\partial}{\partial y}\left(\rho_g * -\frac{k_y}{\mu_g}\left(\frac{\partial p_m}{\partial \mathrm{y}}\right)\right) \qquad (9)$$

From the continuity equation (5)

$$\frac{\partial(\phi\rho)}{\partial t} = -\nabla.\rho\mathbf{v}$$

Accounting for the diffusion (or transfer) of gas from the shale matrix to the natural fractures system, the accumulation term becomes

$$\frac{\partial(\phi\rho)}{\partial t} = -\nabla.\rho\mathbf{v} - q_m \qquad (10)$$

where q_m, in (kg/m^3.s) is the inter-porosity flow model from equation (1), taking place in a form of diffusion. Manipulated to Darcy's expression, q_m is represented as

$$q_m = \frac{\rho_g k_{ma}\alpha_{m\to NF}(p_m - p_{NF})}{\mu_g} \qquad (11)$$

Substituting equations (7), (9), and (11) into (10), the whole equation becomes

$$\frac{\partial p_m}{\partial t}\left(\frac{M}{zRT}\phi_m + \frac{\rho_s M}{V_{std}} * V_{L} * \mathrm{P_L} * \frac{1}{\left(\mathrm{p_m} + \mathrm{P_L}\right)^2}\right)$$

$$= -\left[\frac{\partial}{\partial x}\left(\rho_g * -\frac{k_{ma}}{\mu_g}\left(\frac{\partial p_m}{\partial \mathrm{x}}\right)\right) + \frac{\partial}{\partial y}\left(\rho_g * -\frac{k_{ma}}{\mu_g}\left(\frac{\partial p_m}{\partial \mathrm{y}}\right)\right)\right] - \left[\frac{\rho_g k_{ma}\alpha_{m\to NF}(p_m - p_{NF})}{\mu_g}\right]$$

which simplifies to

$$\frac{\partial p_m}{\partial t}\left(\frac{M}{zRT}\phi_m + \frac{\rho_s M}{V_{std}} * V_{L} * \mathrm{PL} * \frac{1}{\left(\mathrm{p_m} + \mathrm{PL}\right)^2}\right)$$

$$= \frac{\rho_g k_{ma}}{\mu_g} * \frac{\partial^2 \mathrm{p_m}}{\partial x^2} + \frac{\rho_g k_{ma}}{\mu_g} * \frac{\partial^2 \mathrm{p_m}}{\partial y^2} - \left[\frac{\rho_g k_{ma} \alpha_{m \to NF}\left(p_m - p_{NF}\right)}{\mu_g}\right]$$

Dividing the whole equation with the constant gas density, gives

$$\frac{\partial p_m}{\partial t}\left(\phi_m + \frac{\rho_s * RT}{V_{std}} * V_{L} * \mathrm{PL} * \frac{1}{\left(\mathrm{p_m} + \mathrm{PL}\right)^2}\right) = \frac{k_{ma}}{\mu_g} * \frac{\partial^2 \mathrm{p_m}}{\partial x^2} + \frac{k_{ma}}{\mu_g} * \frac{\partial^2 \mathrm{p_m}}{\partial y^2} - \left[\frac{k_{ma} \alpha_{m \to NF}\left(p_m - p_{NF}\right)}{\mu_g}\right] \qquad (12)$$

μ_g is the viscosity of gas; k_{ma} is the matrix apparent permeability which is employed where the gas transport in porous media is in the slip flow regime (gas formations with very low permeability less than 0.001 mD). The flow regime is better explained by the Knudsen number-an expression used to describe different patterns of gas transport in porous media (Zhang, et al., 2017). The Knudsen number for the shale gas reservoir is greater than 0.1, however in this research report, since the mathematical model derived is based on the continuity equation-which does not hold for flow regimes described by a Knudsen number greater than 0.1 (Shen, Li, Xu, & Sun, 2017), slip flow regime and thus the slippage effect is considered in the matrix. Under this condition, the absolute permeability, which is a rock property and not a fluid property (Dandekar, 2013), depends on the reservoir pressure (Guo & Wei, 2015), expressed as

$$k_{ma} = k_l\left(1 + \frac{b}{p_m}\right)$$

where k_l = intrinsic permeability to liquid, and

b = the Klinkenberg slip factor (Pa); although it is a function of pore size and the nature of gas concerned, in this research it is considered constant and is given as

$$b = \frac{4k_l}{2.81708k_l\sqrt{\frac{k_l}{\Phi}}}\sqrt{\frac{\pi RT}{2M}}$$

where T is the reservoir temperature (K). Since only single phase of gas (methane only) is considered in this research, the pressure effect on the gas viscosity and the compressibility factor is negligible and thus the viscosity is constant and the compressibility factor is z = 1.

$\alpha_{m\to NF}$ is the inter-porosity shape factor from the matrix to natural fractures, given as

$$\alpha_{m\to NF} = \frac{A_{mNF}}{L_{NF}}$$

A_{mNF} is interface area between the matrix and the natural fractures per unit volume, and L_{NF} is the characteristic length of natural fracture taken as the natural fracture's average spacing, generally ranging from 0.05 – 10 metres (Jiang & Xu, 2017).

Substituting the values from Table 2.1 and Table 2.2, of all the known parameters into equation (12) gives

$$0.0579\frac{\partial p_m}{\partial t} = 8.319\times10^{-14}\frac{\partial^2 p_m}{\partial x^2} + 8.319\times10^{-14}\frac{\partial^2 p_m}{\partial y^2} - 4.159\times10^{-11}\left(20\times10^6 - p_{NF}\right) \quad (13)$$

Initial boundary: $p_m = p_i,\ t = 0$

Boundary condition: $\frac{\partial p_m}{\partial n}_{\Gamma} = 0,\ t > 0$

4.3 Natural fracture phase

In the natural fractures, only free gas is available, ready for production. Therefore the rate of mass accumulation is

$$\frac{\partial}{\partial t}\left(\phi_{NF}.\rho_g\right)$$

Therefore from the continuity equation (5) and logic from equation (10),

$$\frac{\partial(\phi\rho)}{\partial t} = -\nabla.\rho\mathbf{v}$$

$$\frac{\partial}{\partial t}\left(\phi_{NF}.\rho_g\right) = -\left[\frac{\partial}{\partial x}\left(\rho_g v_x\right) + \frac{\partial}{\partial y}\left(\rho_g v_y\right)\right] + q_m - q_f$$

Where q_f is the inter-porosity flow term from the natural fractures to the hydraulic fractures; it is expressed as

$$q_f = \frac{\rho_g k_{NFa} \alpha_{NF \to HF} (p_{NF} - p_{HF})}{\mu_g} \qquad (14)$$

where $\alpha_{NF \to HF}$ is the inter-porosity shape factor from the natural fractures to hydraulic fractures, given as

$$\alpha_{NF \to HF} = \frac{A_{NF \to HF}}{L_{HF}}$$

q_m in the continuity equation is positive because it contributes/or add to the accumulation of gas in the natural fractures, from the matrix.

The natural fracture continuity equation then becomes

$$\frac{\partial}{\partial t}\left(\phi_{NF} . \frac{p_{NF} M}{zRT}\right) = \frac{\rho_g k_{NF}}{\mu_g} * \frac{\partial^2 p_{NF}}{\partial x^2} + \frac{\rho_g k_{NF}}{\mu_g} * \frac{\partial^2 p_{NF}}{\partial y^2} + \frac{\rho_g k_{ma} \alpha_{m \to NF} (p_m - p_{NF})}{\mu_g} - \frac{\rho_g k_{NF} \alpha_{NF \to HF} (p_{NF} - p_{HF})}{\mu_g}$$

Factoring out the constants gives

$$\frac{\phi_{NF} M}{zRT} . \frac{\partial p_{NF}}{\partial t} = \frac{\rho_g k_{NF}}{\mu_g} * \frac{\partial^2 p_{NF}}{\partial x^2} + \frac{\rho_g k_{NF}}{\mu_g} * \frac{\partial^2 p_{NF}}{\partial y^2} + \frac{\rho_g k_{ma} \alpha_{m \to NF} (p_m - p_{NF})}{\mu_g} - \frac{\rho_g k_{NF} \alpha_{NF \to HF} (p_{NF} - p_{HF})}{\mu_g} \qquad (15)$$

The gas slippage effect is a function of type of gas used to measure permeability of a given rock sample, and according to Klinkenberg's observations, a straight line of positive gradient is obtained for all gases when the permeability of a gas is plotted as a function of a reciprocal mean pressure (Dandekar, 2013). Therefore from Klinkenberg's observations, at high

permeability, which is the case for natural and hydraulic fractures because of decreased pressure relative to pressure in the matrix after desorption, the point in the straight line moves away from the Klinkernberg corrected permeability (Dandekar, 2013). In the natural fracture network, the gas flow pattern is regarded as Darcy flow, and thus the permeability is not adjusted (Zhang, et al., 2017).

Dividing equation (15) by the constant gas density, the overall equation becomes

$$\frac{\phi_{NF}}{p_{NF}}.\frac{\partial p_{NF}}{\partial t} = \frac{k_{NF}}{\mu_g} * \frac{\partial^2 p_{NF}}{\partial x^2} + \frac{k_{NF}}{\mu_g} * \frac{\partial^2 p_{NF}}{\partial y^2} + \frac{k_{ma}\alpha_{m\to NF}(p_m - p_{NF})}{\mu_g} - \frac{k_{NF}\alpha_{NF\to HF}(p_{NF} - p_{HF})}{\mu_g} \quad (16)$$

Again, substituting the values from Table 2.1 and Table 2.2, of all the known parameters into equation (16) gives

$$5 \times 10^{-10}\frac{\partial p_{NF}}{\partial t} = 4.838 \times 10^{-12}\frac{\partial^2 p_{NF}}{\partial x^2} + 4.838 \times 10^{-12}\frac{\partial^2 p_{NF}}{\partial y^2} + 4.159 \times 10^{-11}(20 \times 10^6 - p_{NF}) - 2.419 \times 10^{-12}(20 \times 10^6 - p_{HF}) \quad (17)$$

Initial boundary: $p_{NF} = p_i,\ t = 0$

Boundary condition: $\frac{\partial p_{NF}}{\partial n}_{\Gamma} = 0,\ t > 0$

4.4 Hydraulic fracture phase

Just like in the natural fracture network, flow in the hydraulic fracture network is Darcy flow and thus the Klinkenberg effect employed to adjust the permeability does not form part of the equation. Again recalling from (Dandekar, 2013), that permeability is a rock property and not a fluid property, a rock will retain its measured or known permeability provided the pressure remains constant, hence permeability does not change with the nature of a fluid.

The flow in the hydraulic fracture is considered one dimensional (1-D) flow, therefore the continuity equation is

$$\frac{\partial}{\partial t}(\phi_{HF}.\rho_g) = -\left[\frac{\partial}{\partial y}(\rho_g v_y)\right] + q_f - q_w \qquad (18)$$

where q_w is the inter-porosity flow term from the main hydraulic fractures to the horizontal well, expressed as

$$q_w = \frac{2\pi\rho_g k_{HF}(p_{HF}-p_w)}{\Delta x\Delta y\mu_g \ln\left(\frac{r_e}{r_w}\right)} \text{ (at the grid intersect with the wellbore)} \qquad (19)$$

$r_e = 0.14\sqrt{\Delta x^2 + \Delta y^2}$

Δx and Δy are the widths of the grid at which the hydraulic fractures intersect with the wellbore (Zhang, et al., 2017).

Substituting equation (19) into (18), the hydraulic fractures continuity equation becomes

$$\frac{\phi_{HF}M}{zRT}.\frac{\partial p_{HF}}{\partial t} = \frac{\rho_g k_{HF}}{\mu_g} * \frac{\partial^2 \mathrm{p_{HF}}}{\partial y^2} + \frac{\rho_g k_{NF}\alpha_{NF\to HF}(p_{NF}-p_{HF})}{\mu_g} - \frac{2\pi\rho_g k_{HF}\left(p_{HF}-p_w\right)}{\Delta x\Delta y\mu_g \ln\left(\frac{r_e}{r_w}\right)}$$

And again, dividing this equation by the constant gas density, the overall equation becomes

$$\frac{\phi_{HF}}{p_{HF}}.\frac{\partial p_{HF}}{\partial t} = \frac{k_{HF}}{\mu_g} * \frac{\partial^2 \mathrm{p_{HF}}}{\partial y^2} + \frac{k_{NF}\alpha_{NF\to HF}(p_{NF}-p_{HF})}{\mu_g} - \frac{2\pi k_{HF}\left(p_{HF}-p_w\right)}{\Delta x\Delta y\mu_g \ln\left(\frac{r_e}{r_w}\right)} \qquad (20)$$

Once again substituting the known values from Table 2.1 and Table 2.2 into equation (20) gives

$$0.05\times10^{-6}\frac{\partial p_{HF}}{\partial t} = 774.0392\times10^{-9}\frac{\partial^2 p_{HF}}{\partial y^2} + 2.419\times10^{-12}(20\times10^6 - p_{HF}) - 2.640\times10^{-4} \qquad (21)$$

Initial boundary: $p_{HF} = p_i,\ t = 0$

Outer boundary condition: $\frac{\partial p_m}{\partial n}_{\Gamma} = 0;\ t > 0$

Inner boundary condition: $q_w = \frac{2\pi\rho_g k_{HF}(p_{HF}-p_w)}{\Delta x\Delta y\mu_g \ln\left(\frac{r_e}{r_w}\right)};\ t > 0$

Chapter 5: Solution to the models developed

In this research report a method known as the finite difference method (FDM) is employed to solve the three derived differential equations; this method is known as one of the simplest and of the oldest methods to solve differential equations (Bui, 2009). The principle of this method is that it is utilized to approximate derivatives in the partial differential equation by linear combinations of function values at grid points, especially boundary value equations; the differential equations are approximated with difference equations, which approximate the derivatives in finite differences.

The partial differential equations are solved numerically at predefined set of discrete points (also called nodal points) in the structured grid, starting by identifying the grid points of the given domain, which is the first step in the finite difference approximation called discretization of the domain. Here the discrete points are placed uniformly and connected by straight lines which gives the required grid, and the controlled partial equations are approximated or discretized at the identified grid points. Thereafter, the algebraic equations obtained by approximation or discretization are solved using direct or iterative methods; here the iterative method is used to approximate the derivatives in finite differences.

Firstly the hydraulic fracture phase equation is solved to find p_{HF}, which is substituted into the natural fracture equation to find p_{NF}; finally after obtaining both the values of p_{HF} and p_{NF}, they are substituted into the matrix equation to get p_m.

5.1 Hydraulic fracture phase

The derived hydraulic fracture model

$$0.05 \times 10^{-6} \frac{\partial p_{HF}}{\partial t} = 774.0392 \times 10^{-9} \frac{\partial^2 p_{HF}}{\partial y^2} + 2.419 \times 10^{-12}(20 \times 10^6 - p_{HF}) - 2.640 \times 10^{-4}$$

Initial boundary: $p_{HF} = p_i = 20 \times 10^6\ Pa, y = 0,\ t \geq 0$

Outer boundary condition: $\frac{\partial p_m}{\partial n}_{\Gamma} = 0;\ t > 0$

Inner boundary condition: $p_{HF} = p_w = 5 \times 10^6\ Pa,\ t > 0$

is of the general diffusion equation in one dimension (1-D), also known as the heat equation, describing the behaviour or distribution of pressure in a given region over time, resulting from the movement of gas. It can be represented as

$$\frac{\partial p(y,t)}{\partial t} = c\frac{\partial^2 p}{\partial y^2} + F(p,y)$$

where $p(y,t)$ is the unknown function; c is a known constant from the ratio of permeability to the gas viscosity, and $F(p,y)$ is taken as the collective diffusion coefficient for pressure at location *y*.

Derivatives are approximated with difference equations as below:

$$\frac{\partial p}{\partial t} \approx \frac{p_i^{k+1} - p_i^k}{\Delta t}$$

$$\frac{\partial^2 p}{\partial y^2} \approx \frac{p_{i+1}^k - 2p_i^k + p_{i-1}^k}{\Delta y^2}$$

Therefore the approximation of the hydraulic fracture differential equation is

$$\frac{p_i^{k+1} - p_i^k}{\Delta t} = c\frac{p_{i+1}^k - 2p_i^k + p_{i-1}^k}{\Delta y^2} + F(p_k, y_i)$$

Explicitly

$$p_i^{k+1} = p_i^k + c\frac{\Delta t}{\Delta y^2}\left(p_{i+1}^k - 2p_i^k + p_{i-1}^k\right) + \Delta t\left[2.419 \times 10^{-12}\left(20 \times 10^6 - p_i^k\right) - 2.640 \times 10^{-4}\right]$$

5.2 Natural fracture phase

The derived natural fracture differential model is also of the general diffusion or heat equation, however in two dimensions (2-D).

$$5 \times 10^{-10}\frac{\partial p_{NF}}{\partial t} = 4.838 \times 10^{-12}\frac{\partial^2 p_{NF}}{\partial x^2} + 4.838 \times 10^{-12}\frac{\partial^2 p_{NF}}{\partial y^2} + 4.159 \times 10^{-11}(20 \times 10^6 - p_{NF}) - 2.419 \times 10^{-12}(20 \times 10^6 - p_{HF})$$

Initial boundary: $p_{NF} = p_i = 20 \times 10^6\ Pa,\ t = 0$

Outer boundary condition: $p_{NF} = p_i = 20 \times 10^6\ Pa$

$$\frac{\partial p_{NF}}{\partial n}_{\Gamma} = 0, \qquad t > 0$$

Inner boundary condition: $p_{NF} = p_w = 5 \times 10^6\ Pa$

Considering 2-D the general diffusion equation in this case will therefore be represented as

$$\frac{\partial p(y,t)}{\partial t} = c\left(\frac{\partial^2 p}{\partial x^2} + \frac{\partial^2 p}{\partial y^2}\right) + F(p,x,y)$$

Approximation of the derivatives by difference equations is the same as in the hydraulic fracture phase

$$\frac{\partial p}{\partial t} \approx \frac{p_i^{l+1} - p_i^l}{\Delta t}$$

$$\frac{\partial^2 p}{\partial x^2} \approx \frac{p_{i+1}^l - 2p_i^l - p_{i-1}^l}{\Delta x^2}$$

$$\frac{\partial^2 p}{\partial y^2} \approx \frac{p_{i+1}^l - 2p_i^l - p_{i-1}^l}{\Delta y^2}$$

Therefore the approximation of the derivatives of the natural fracture differential system is

$$\frac{p_{i,j}^{l+1} - p_{i,j}^l}{\Delta t} = c\left(\frac{p_{i,j+1}^l - 2p_i^l + p_{i,j-1}^l}{\Delta x^2} + \frac{p_{i,j+1}^l - 2p_{i,j}^l + p_{i,j-1}^l}{\Delta y^2}\right) + F(p_{k,l}, x_{i,j}, y_{i,j})$$

Explicitly

$$p_{i,j}^{l+1} = p_{i,j}^l + c\frac{\Delta t}{\Delta x^2}\left(p_{i,j+1}^l - 2p_{i,j}^l + p_{i,j-1}^l\right) + c\frac{\Delta t}{\Delta y^2}\left(p_{i,j+1}^l - 2p_{i,j}^l + p_{i,j-1}^l\right) + \Delta t\left[4.159 \times 10^{-11}\left(20 \times 10^6 - p_{i,j}^l\right) - 2.419 \times 10^{-12}\left(20 \times 10^6 - p_i^k\right)\right]$$

5.3 Matrix phase

Since the differential system of the matrix phase

$$0.0579\frac{\partial p_m}{\partial t} = 8.319 \times 10^{-14}\frac{\partial^2 \mathrm{p_m}}{\partial x^2} + 8.319 \times 10^{-14}\frac{\partial^2 \mathrm{p_m}}{\partial y^2} - 4.159 \times 10^{-11}\left(20 \times 10^6 - p_{NF}\right)$$

Initial boundary: $p_m = p_i = 20 \times 10^6\ Pa,\ t = 0$

Outer boundary condition: $p_m = p_i = 20 \times 10^6\ Pa$

$$\frac{\partial p_m}{\partial n}_{\Gamma} = 0, \qquad t > 0$$

Inner boundary condition: $p_m = p_w = 5 \times 10^6\ Pa$

is of the same form as the natural fracture phase, the general diffusion equation in 2-D also applies in the matrix differential system, and so are the finite difference equations; therefore the approximation of the derivatives of the matrix differential system is

$$\frac{p_{i,j}^{n+1} - p_{i,j}^{n}}{\Delta t} = c\left(\frac{p_{i,j+1}^{n} - 2p_{i}^{n} + p_{i,j-1}^{n}}{\Delta x^2} + \frac{p_{i,j+1}^{n} - 2p_{i,j}^{n} + p_{i,j-1}^{n}}{\Delta y^2}\right) + F\left(p_{n,l}, x_{i,j}, y_{i,j}\right)$$

Explicitly

$$p_{i,j}^{n+1} = p_{i,j}^{n} + c\frac{\Delta t}{\Delta x^2}\left(p_{i,j+1}^{n} - 2p_{i,j}^{n} + p_{i,j-1}^{n}\right) + c\frac{\Delta t}{\Delta y^2}\left(p_{i,j+1}^{n} - 2p_{i,j}^{n} + p_{i,j-1}^{n}\right) - \Delta t\left[4.159 \times 10^{-11}\left(20 \times 10^{6} - p_{i,j}^{l}\right)\right]$$

Chapter 6: Analysis of the results

The algorithm of the model was developed and solved using MATLAB. The colour change in the graphs presented below represents the change in the intensity of pressure with respect to time and location of the gas. The pressure decrease or pressure drop with respect to time starts from the initial reservoir pressure until a certain pressure is reached, depending on the coefficient of the pressure distribution function with respect to the location of the gas flow; the coefficient is the ratio of rock permeability to fluid (gas) viscosity. At bigger coefficients of the pressure distribution function with respect to the location of gas flow, the pressure drop from the initial reservoir pressure towards the bottom-hole pressure is steeper compared to at smaller coefficients, which the area under the graph indicates the impulse or force exerted on the gas flow along the reservoir, per unit area of flow of released adsorbed gas; this means that at bigger coefficients only a small amount of released adsorbed gas is produced, agreeing with the numerical model proposed by (Zhang, et al., 2017) whose model matched the field data they used to validate their model. From the known constant c, three other c values were picked or assumed to show the effect of permeability on pressure distribution.

The graphs below are graphs generated from executing the algorithms of the derived triple-porosity model on MATLAB.

6.1 Hydraulic fracture network

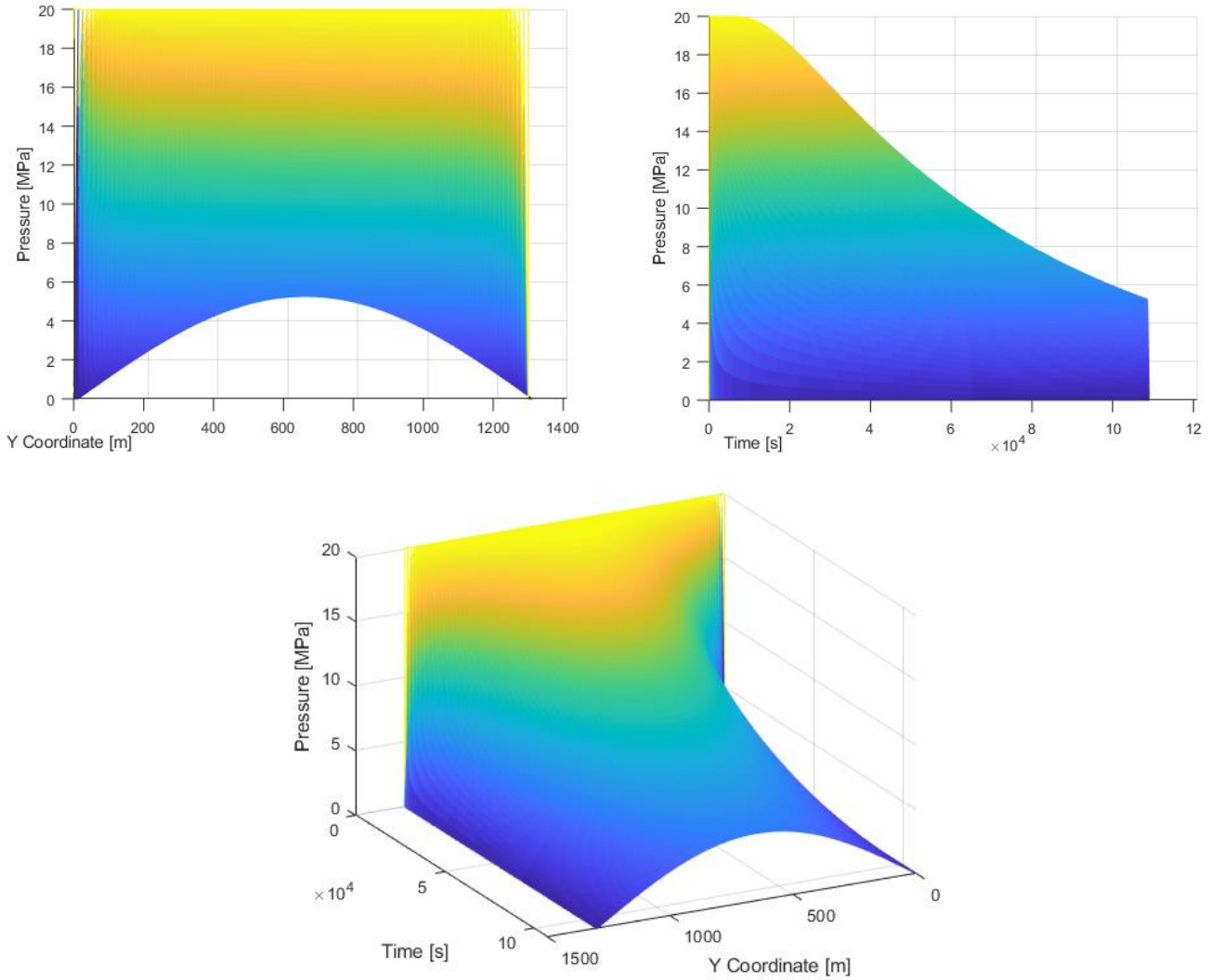


Figure 6. 1: Pressure distribution with respect to time and location of the gas in the hydraulic fracture phase, where the known constant c is 2.5.

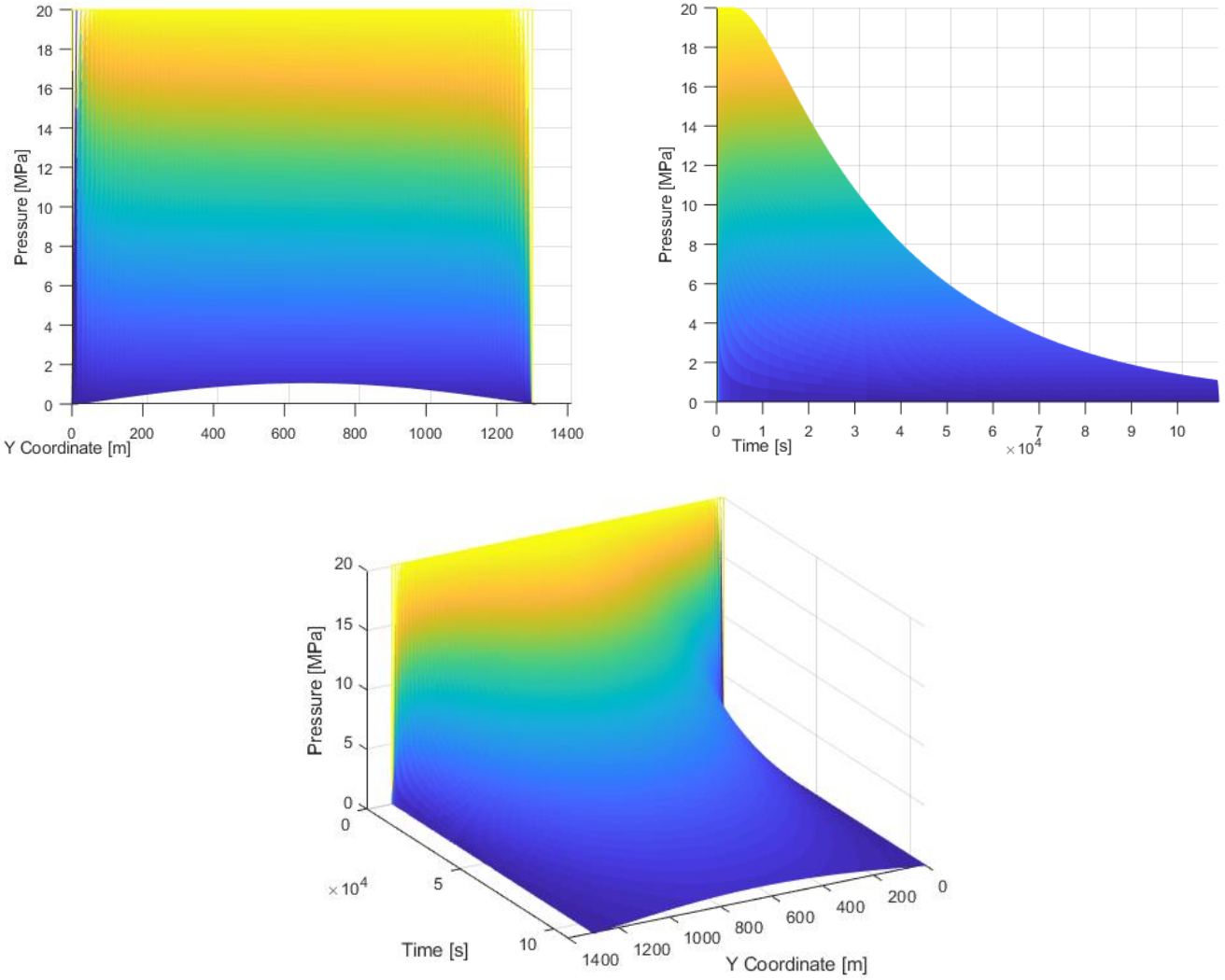


Figure 6. 2: Pressure distribution with respect to time and location of the gas in the hydraulic fracture phase, where the known constant c is 5.

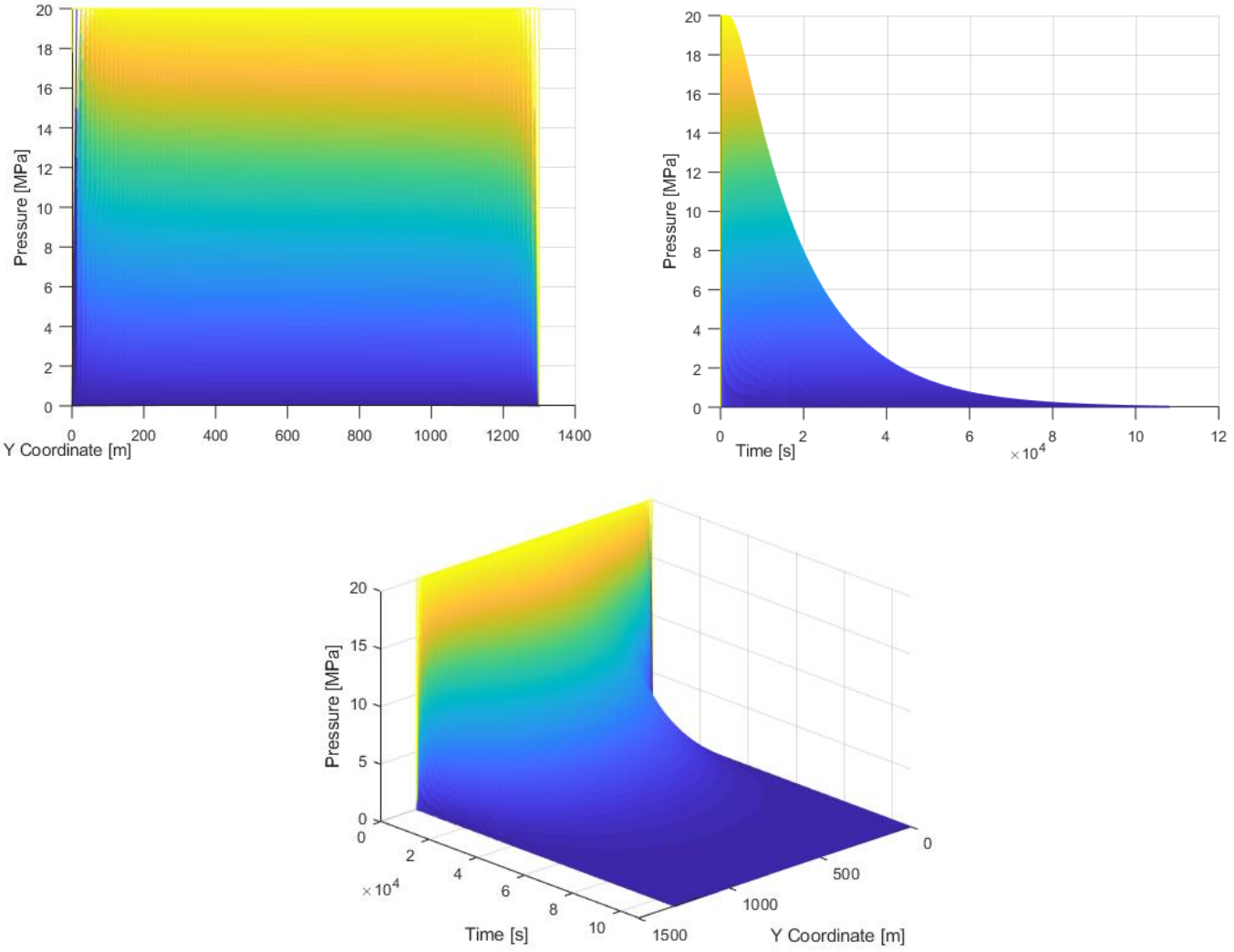


Figure 6. 3: Pressure distribution with respect to time and location of the gas in the hydraulic fracture phase, where the known constant c is 10.

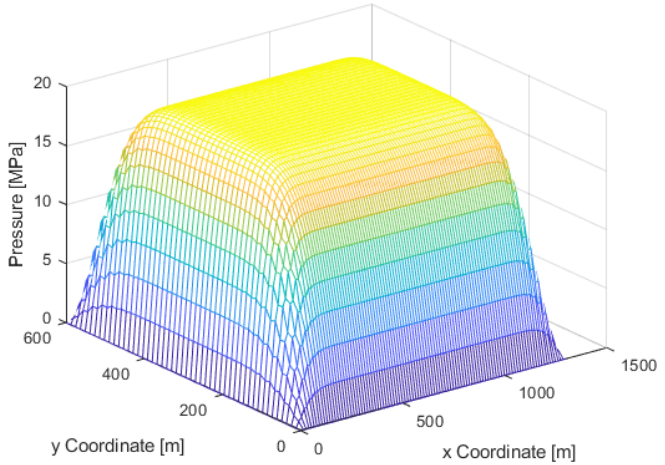
The graphs above describe the pressure increase as the gas changes position along the hydraulic fracture network until it reaches a maximum at approximately half the length of the hydraulic fracture network, then pressure starts to decrease until it stabilizes at a certain value at just the beginning of the production well, where the gas starts to come out of the shale reservoir entering the wellbore; this behaviour agrees with the analytical model by (Berawala, 2015) simulated on FORTRAN compiler, describing the pressure variation with distance in the fracture network.

At bigger coefficients of the pressure distribution function with respect to the location of gas flow, though it is difficult to see the pressure change with respect to the location of gas flow, the pressure change is only significant just after gas flow begins, and then drastically change to a constant pressure; this means that at high rock permeability and/or low gas viscosity, pressure with respect to flow equilibrates or stabilizes quickly, which agrees with Darcy's law (Dandekar, 2013); at this point the gas flow rate will also decrease drastically and stabilizes at a constant flow rate, thus decreasing the production rate.

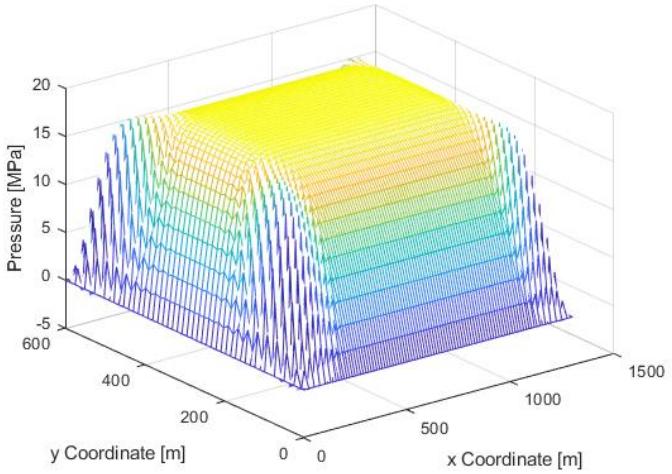
6.2 Natural fracture network and the matrix phase

The pressure behaviour in the natural fracture network and the matrix phase is similar, in the sense that when production begins and gas starts flowing pressure increases and fluctuates sharply, and then stabilizes at a constant value as production time progresses; as the end of the production time approaches, pressure fluctuation begins again and pressure decreases to a constant value at the end of the production time. Note, a zero pressure does not necessarily mean the pressure is zero, but it is at a constant value of the system when production has not yet started, same as the negative pressure, which means the pressure decreases below the constant pressure of the system before production has started.

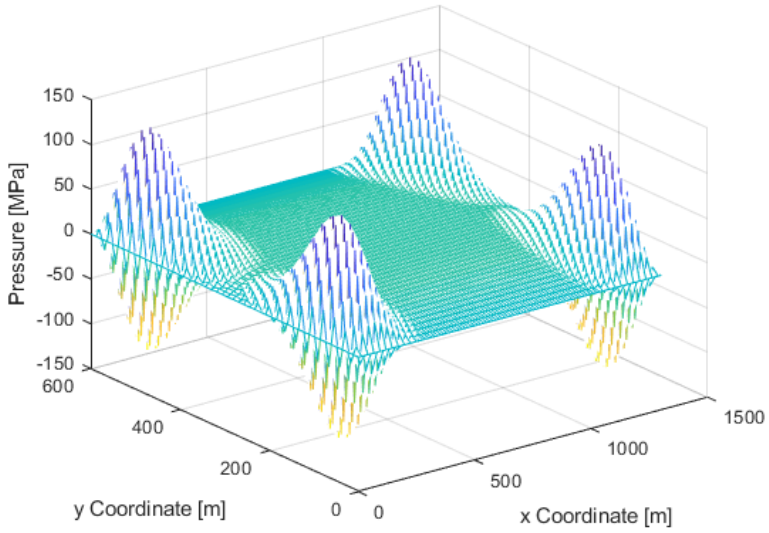
Figure 6.4 and 6.5 below are the natural fracture network and the matrix phase results, describing the above explained behaviour.


Pressure [MPa]
20
15
10
5
0
600
400
200
0
y Coordinate [m]
0
500
1000
1500
x Coordinate [m]

(a)

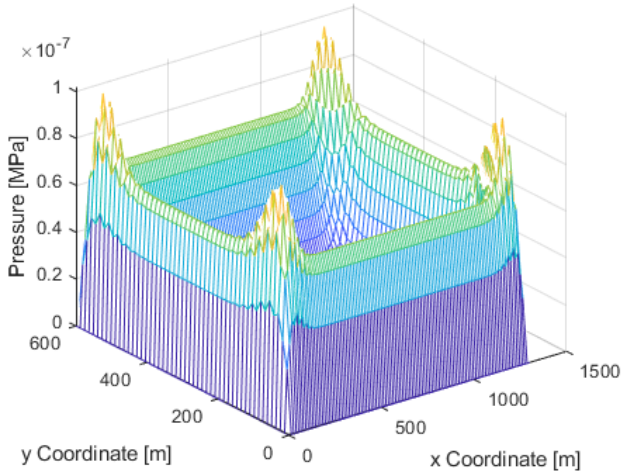

Pressure [MPa]
20
15
10
5
0
-5
600
400
200
0
y Coordinate [m]
0
500
1000
1500
x Coordinate [m]

(b)

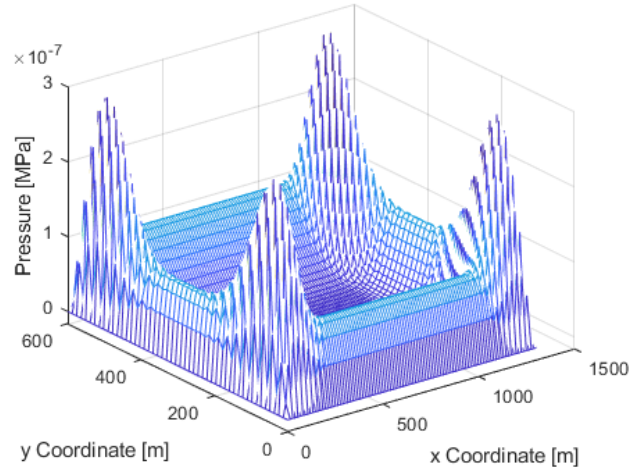


(c)

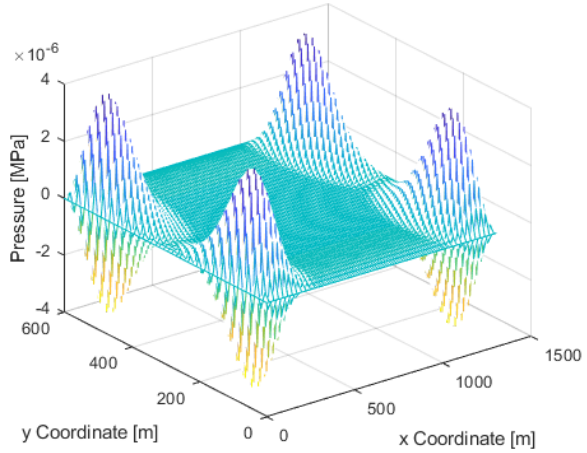
Figure 6. 4: Pressure distribution in the natural fracture with respect to gas flow at different increasing time steps shown by (a), (b) and (c), respectively.


×10^-7
1
0.8
0.6
0.4
0.2
0
Pressure [MPa]
600
400
200
0
y Coordinate [m]
0
500
1000
1500
x Coordinate [m]

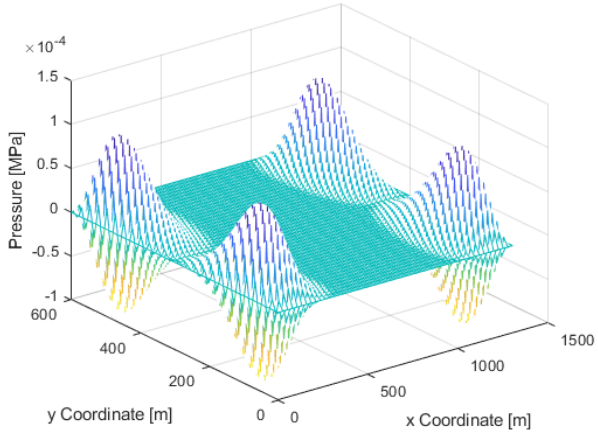
(a)


×10^-7
3
2
1
0
Pressure [MPa]
600
400
200
0
y Coordinate [m]
0
500
1000
1500
x Coordinate [m]

(b)



(c)



(d)

Figure. 6.5: Pressure distribution in the matrix phase with respect to gas flow at different increasing time steps shown by (a), (b), (c), and (d), respectively.

The pressure fluctuation in the matrix phase, however, is sharper than the pressure fluctuation in the natural fracture network; this is explained by the size difference between the matrix porosity and the natural fracture porosity, which affects the area of flow, so is the production rate. The permeability and the porosity size of the matrix are significantly smaller than of the natural fracture, thus pressure fluctuates (as it increases or decreases) sharper in the matrix than in the natural fracture, which is also true according to Darcy's law for natural fractures and according to the gas slippage effect in the matrix.

Chapter 7: Conclusions and future work

The triple-porosity continuum was established to incorporate the matrix phase, the natural fracture network, and the hydraulic fracture network. Three mathematical models describing the natural gas (methane) behaviour during gas production were modelled and simulated in MATLAB, of their algorithm is presented in Appendix A at the end of the report. The results generated by the developed model agree with previously developed and field data validated models, which substantiate the reliability of the model developed in this research report.

Permeability of shale gas reservoirs, which has control over the initial reservoir pressure (Dandekar, 2013), has a significant effect on the gas production rate, especially on the hydraulically induced fractures; a low permeability is preferable when a higher production rate is desired, however a too low permeability will decrease the production rate also. Therefore, when hydraulic fracturing is performed, it is important that a permeability achieving an optimal production rate is determined; a sensitivity analysis on the hydraulic fracture permeability with gas production rate is thus recommended, which was not covered in the scope of this research project.

Nomenclature

	Units	Symbol
Natural fracture		NF
Hydraulic fracture		HF
Reservoir thickness	m	h
Reservoir length,	m	L
Reservoir breadth	m	w
Klinkenberg coefficient	MPa	b
Matrix porosity,		ϕ_m
Natural fracture porosity,		ϕ_{NF}
Hydraulic fracture porosity,		ϕ_{HF}
Compressibility factor,		Z
Normal direction		n
Wellbore radius,	m	r_w
Initial reservoir pressure	Pa	p_i
Bottom-hole pressure	Pa	p_w
Matrix pressure	Pa	p_m
Natural fracture pressure	Pa	p_{NF}
Hydraulic fracture pressure	Pa	p_{HF}
Langmuir pressure	Pa	p_L
Mass flux of the adsorbed gas	[kg/(m^3. s)]	q_{ad}
Inter-porosity flow from matrix to natural fracture	[kg/(m^3. s)]	q_m
Inter-porosity flow from natural fracture to hydraulic fracture	[kg/(m^3. s)]	q_{NF}
Reservoir temperature	K	T
Langmuir volume,	m^3/kg	V_L
Apparent permeability	m^2	k_a
Intrinsic permeability	m^2	k_l
Absolute permeability of matrix	m^2	k_{mi}
Apparent permeability of matrix	m^2	k_{ma}
Absolute permeability of natural fracture	m^2	k_{NF}
Absolute permeability of hydraulic fracture	m^2	k_{HF}
Molecular weight of gas	kg/mol	M
Interface area per unit volume of rock	m^{-1}	$A_{m\rightarrow NF}$
Interface area per unit volume of rock	m^{-1}	$A_{NF\rightarrow HF}$
Gas Viscosity	cP	μ_g
Flow term from HF to the horizontal to the horizontal well	[kg/(m^3 .s)]	q_w
Universal gas constant	[Pa m^3/(kmol .K)]	R
Effective radius of the grid where HF intersects with wellbore	m	r_e
Gas density	(kg/m^3)	ρ
Time	(s)	t
Langmuir volume	(m^3/m^3)	V_L

Adsorbed gas content	(m^3/m^3)	V_E

References

[1] Alahmadi, H. (2010). *A Triple-porosity model for fractured horizontal wells.* Hasan Ali H Alahmadi .

[2] Berawala, D. (2015). Modelling of gas production from tight shale formations*: An innovative approach.* Dhruvit Satishchandra Berawala and Dr. Jann Rune Ursin.

[3] Bui, T. (2009). *Explicit and Implicit Methods In Solving Differential Equations.* Timothy Bui.

Campbell, S., & Mielke, P. &. (2016). *Geothermal energy from the Main Karoo Basin? New insights from borehole KWV-1 (Eastern Cape, South Africa).* The Author(s).

[4] Chevron (Director). (2014). *Chevron's Hydraulic Fracturing Process: Applying Technology With Care* [Motion Picture]. North America.

[5] Dandekar, A. (2013). *Petroleum reservoir rock and fluid properties* (2nd ed.). Taylor & Francis Group.

[6] Ezekwe, N. (2011). Double porosity model. In *Petroleum reservoir engineering practice* (pp. 502-503). Pearson Educatio, Inc.

[7] Geel, C., Schulz, H., Booth, P., & deWit, M. &. (2013). Shale gas characteristics of Permian black shales in South Africa: results from recent drilling in the Ecca Group (Eastern Cape). *Energy Procedia*, 256-265.

[8] Guo, C., & Wei, M. &. (2015). Modeling of Gas Production from Shale Reservoirs Considering Multiple Transport Mechanisms. *PLos One: A peer-reviewed, open access journal, 10*(12).

[9] Herbas, P. (2015). Advanced production data analysis in naturally fractured reservoirs*.* Campinas.

[10] Industry, A. O. (2017). *Hydraulic Fracturing: Unlocking America's Natural Gas Resources.* America's Oil and Natural Gas Industry.

[11] Jiang, R., & Xu, J. &. (2017). Production forecast of fractured shale gas reservoir considering multi-scale gas flow. *Journal of Petroleum Exploration and Production Technology, 7*(4), 1071-1083.

[12] Lee, J. (2015). *Conventional vs. unconventional.* Jessica Lee.

[13] Mohammadi, H., & Manshad, A. &. (2012). A reservoir simulation approach for modeling of naturally fractured reservoirs. *Egyptian Journal of Petroleum*, 125-133.

[14] Montgomery, C. (2013). *Fracturing Fluid Components .* Montgomery.

[15] Nelson, R. (2001). *Geologic analysis of naturally fractured reservoirs .* Butterworth-Heinemann.

[16] Rangel-German, E. &. (2003). Matrix-fracture transfer functions for partially and completely immersed fractures. Proceedings, Twenty-Eighth Workshop on Geothermal Reservoir Engineering

[17] Ryan, P. &. (1978). *Basin analysis of the ecca and lowermost beaufort beds and associated coal, uranium and heavy mineral beach sand occurrences.* University of the Witwatersrand, Johannesburg.

[18] Scally, P. (2012). Fracking comes to Southwest China. *GoKunming Article*, 1.

[19] Shen, W., Li, X., Xu, Y., & Sun, Y. &. (2017). Gas Flow Behavior of Nanoscale Pores in Shale Gas Reservoirs. *Energies article*, 1-12.

[20] Tanikawa, W. &. (2006). *Klinkenberg effect for gas permeability and its comparison to water permeability for porous sedimentary rocks.* Author(s).

[21] Wang, F., Reed, R., & John, A. &. (2009). Pore networks and fluid flow in gas shales. *Society of Petroleum Engineers Journal Article*, 1-8.

[22] Wang, J., Luo, H., Liu, H., Lin, J., & Li, L. &. (2016). Influences of adsorption/desorption of shale gas on the apparent properties of matrix pores. *Petroleum Exploration and Development*, 158-165.

[23] Wang, L., Torres, A., Xiang, L., Fei, X., & Naido, A. &. (2015). *A Technical Review on Shale Gas Production and Unconventional Reservoirs Modeling.* Science Research Publishing Inc.

[24] Warren, J. &. Root, P. (1963). The Behavior of Naturally Fractured Reservoirs. *Society of Petroleum Engineers Journal*, 245-255.

[25] Wei, M., Liu, J., & Elsworth, D. &. (2018). Triple-Porosity Modelling for the Simulation of Multiscale Flow Mechanisms in Shale Reservoirs. *Wiley Research Article*, 1-11.

[26] Welty, J., Wicks, C., & Wilson, R. &. (2008). Conservation of Mass: Control-Volume Approach. In *Fundamentals of Momentum, Heat, and Mass Transfer* (pp. 34-35). John Wiley & Sons, Inc.

[27] Yao, J., Wang, W., & Sun, H. &.-H. (2015). Influence of gas transport mechanisms on the productivity of multi-stage fractured horizontal wells in shale gas reservoirs. *Petroleum Science*, 664-673.

[28] Zhang, W., Xu, J., Jiang, R., Cui, Y., Qiao, J., & Kang, C. &. (2017). Employing a quad-porosity numerical model to analyze the productivity of shale gas reservoir. *Journal of Petroleum Science and Engineering, 157*, 1046-1055.

Appendix A: Developed triple-porosity model algorithm, simulated using MATLAB.

```
clear;clc;

%=========================================================================
%----------------------------Hydraulic fracture network-------------------------
%=========================================================================

%Length of the hydraulic fracture network
L = 1300;                               % length in metres
%Number of Nodes
Nodes = 100;
%Known Constant c
c = 774.039*10^-9;
%Time taken for Gas flow in the hydraulic fracture network
Time = 30*60^2;                         % in seconds
%discretize y our space
%starts at 0, increment to L, and the length of the vector is Nodes
y_vec = linspace(0,L,Nodes);
dy = y_vec(2)-y_vec(1);                 %

%discretize time
dt = 0.5*(dy^2)/(2*c);                  %still to look this up
t_vec = 0:dt:Time;

%Allocate memory for pressure results

Press_HF = zeros(length(y_vec),length(t_vec));

%Initial conditions for pressure of the pipe

Press_HF(:,1) = 20*10^6;                        %Pressure at x >= 0 , t = 0;

%Excplicitly
for tdx = 1:length(t_vec)-1                     %integrates tdx +1
    for idy = 2:length(y_vec)-1
        Press_HF(idy,tdx+1) = Press_HF(idy,tdx)...
            +c*(dt/(dy^2))*(Press_HF(idy+1,tdx)-2*Press_HF(idy,tdx)...
            +Press_HF(idy-1,tdx))...
            +dt*(2.419*10^(-12)*(20*10^6 -Press_HF(idy,tdx))-2.640*10^-4);
    end
end

%=========================================================================
%-----------------------------Natural fracture network-------------------------
%=========================================================================
W=600;
x_nodes=50;
x_vec=linspace(0,W,x_nodes);
dx=x_vec(2)-x_vec(1);
```

```
Press_NF = zeros(length(x_vec),length(y_vec),length(t_vec));

Press_NF(:,:,1) = 20*10^6;                    % Pressure at x,y>= 0 ,t = 0;
%pressure equation ---  remember Pik already exists in the Press_HF matrix

for tdx = 1:length(t_vec)-1                     %integrates tdx +1
    for idy = 2:length(y_vec)-1
        for idx = 2:length(x_vec)-1
           Press_NF(idx,idy,tdx+1) = Press_NF(idx,idy,tdx)...
           +c*dt*(1/(dx^2))*(Press_NF(idx+1,idy,tdx)...
           -2*Press_NF(idx,idy,tdx)+Press_NF(idx-1,idy,tdx))...
           +c*dt*(1/(dy^2))*(Press_NF(idx,idy+1,tdx)...
           -2*Press_NF(idx,idy,tdx)+Press_NF(idx,idy-1,tdx))...
           +dt*(4.159*10^(-11)*(20*10^6-Press_NF(idx,idy,tdx))...
           -2.149*10^(-12)*(20*10^6-Press_HF(idy,tdx)));
        end
    end
end

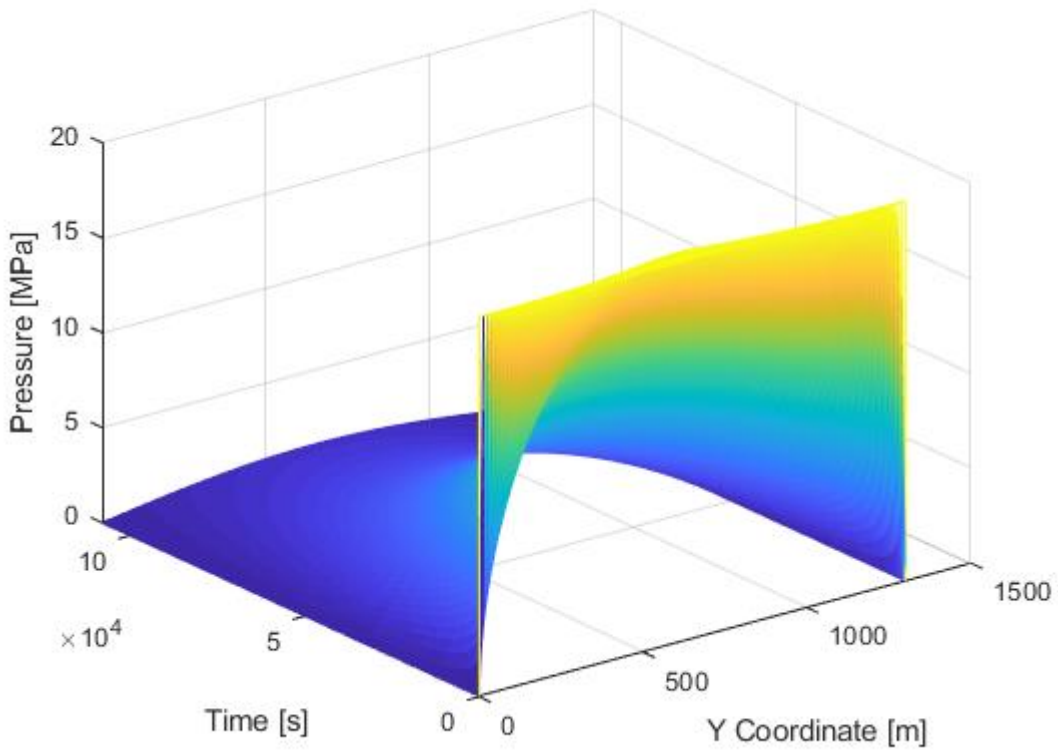
%=========================================================================
%---------------------------------Matrix phase-----------------------------------
%=========================================================================
Press_M = zeros(size(Press_NF));
for tdx = 1:length(t_vec)-1                     %integrates tdx +1
    for idy = 2:length(y_vec)-1
        for idx = 2:length(x_vec)-1
           Press_M(idx,idy,tdx+1) = Press_M(idx,idy,tdx)...
           +c*dt*(1/(dx^2))*(Press_M(idx+1,idy,tdx)...
           -2*Press_M(idx,idy,tdx)+Press_M(idx-1,idy,tdx))...
           +c*dt*(1/(dy^2))*(Press_M(idx,idy+1,tdx)...
           -2*Press_M(idx,idy,tdx)+Press_M(idx,idy-1,tdx))...
           +dt*(4.159*10^(-11)*(20*10^6-Press_NF(idx,idy,tdx)));
        end
    end
end

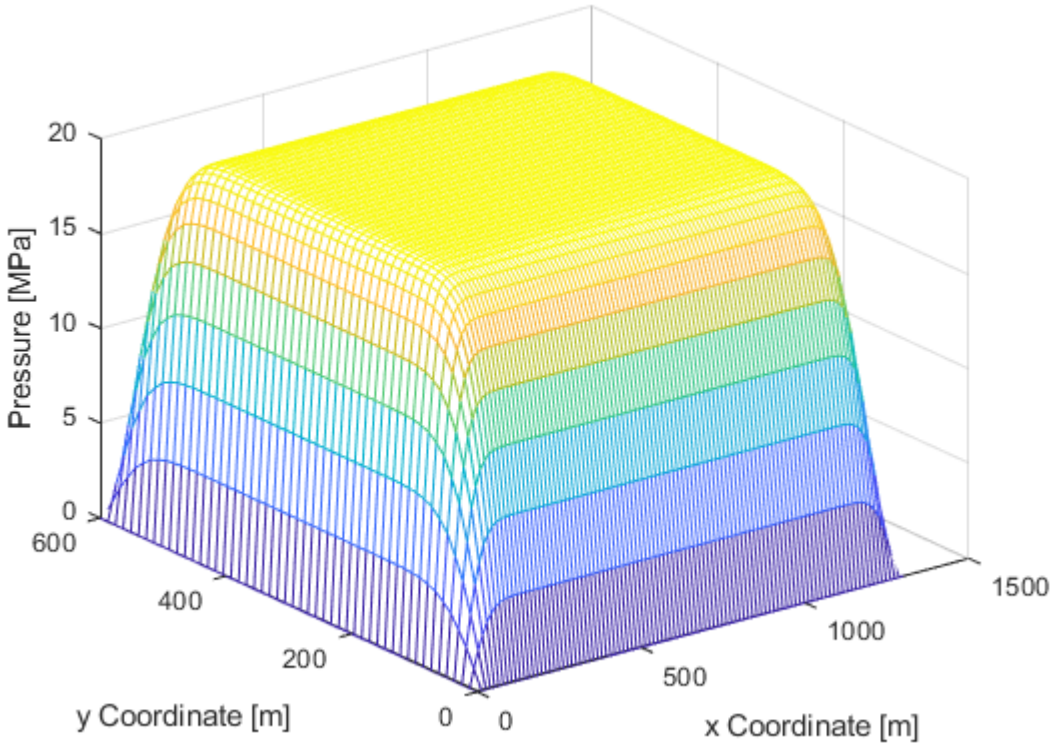
%=========================================================================
%----------------------------Plotting the results-------------------------
%=========================================================================

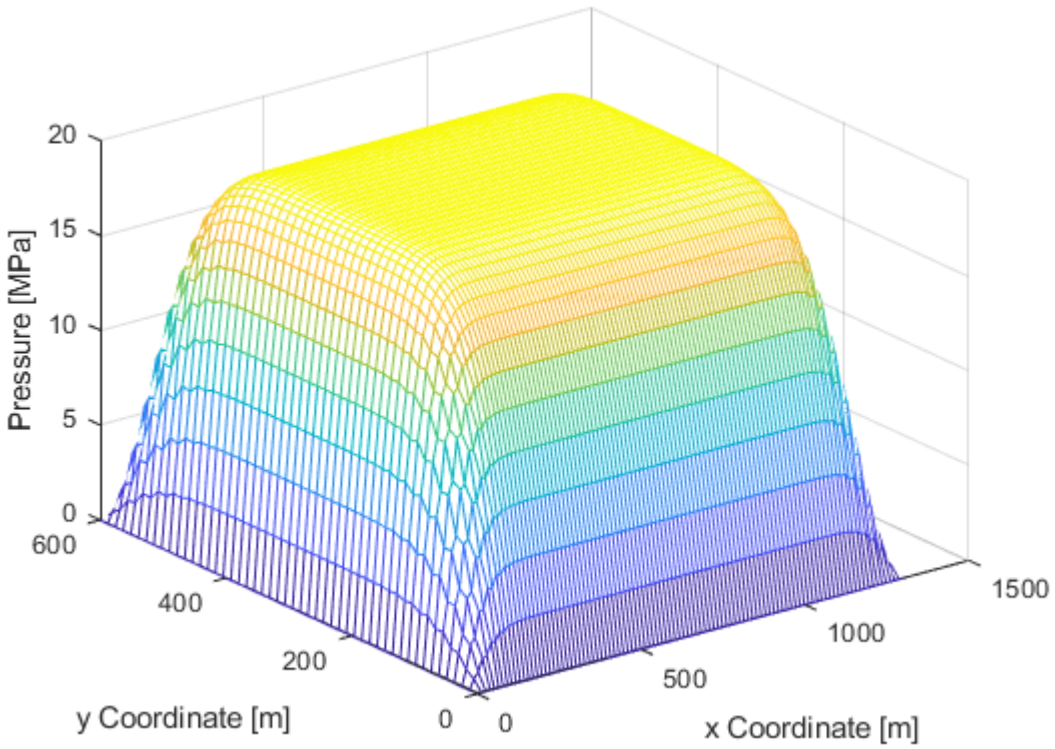
%-------------------------------Hydraulic Fracture network-------------------------
[tt,yy] = meshgrid(t_vec,y_vec);
mesh(yy,tt,Press_HF./10^6)
xlabel('Y Coordinate [m]')
ylabel('Time [s]')
zlabel('Pressure [MPa]')

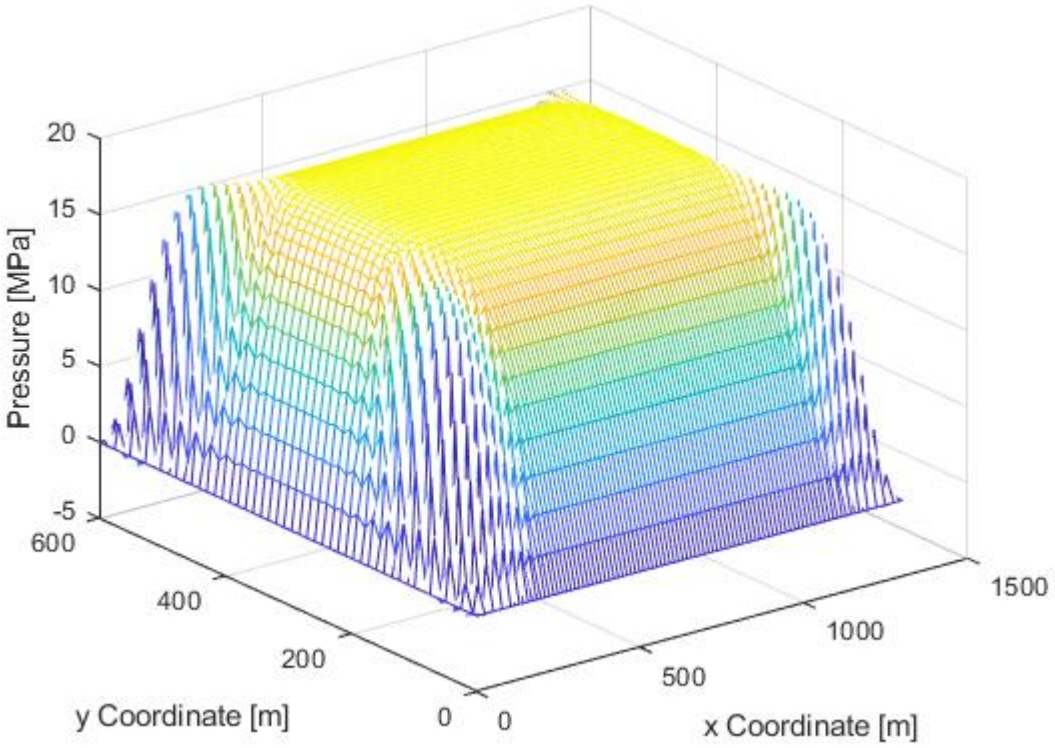
%-------------------------------Natural Fracture network-------------------------
n=25;
for i = 1 : 1: 5
    Figure
    [xx,yy1] = meshgrid(x_vec,y_vec);
    mesh(yy1,xx,Press_NF(:,:,i*n)'./10^6)
    xlabel('x Coordinate [m]')
    ylabel('y Coordinate [m]')
    zlabel('Pressure [MPa]')
 end
```

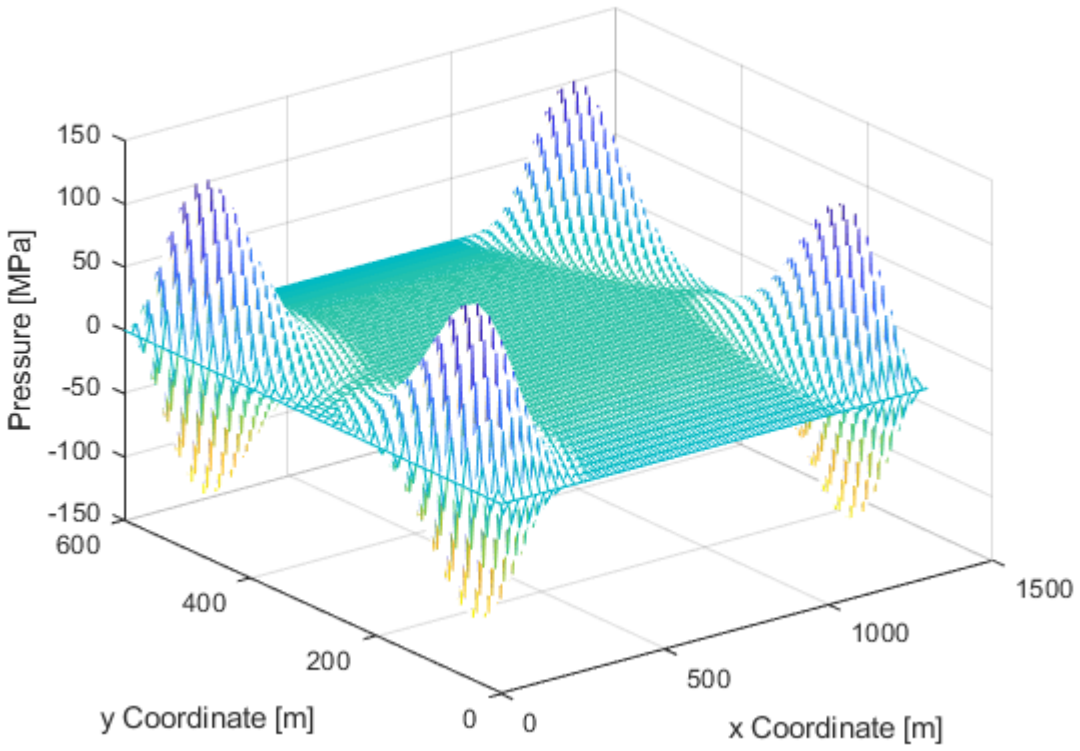
```
%--------------------------------Matrix phase-------------------------
n=25;
for i = 1 : 1: 5
    Figure
    [xx,yy1] = meshgrid(x_vec,y_vec);
    mesh(yy1,xx,Press_M(:,:,i*n)'./10^6)
    xlabel('x Coordinate [m]')
    ylabel('y Coordinate [m]')
    zlabel('Pressure [MPa]')
 end
```

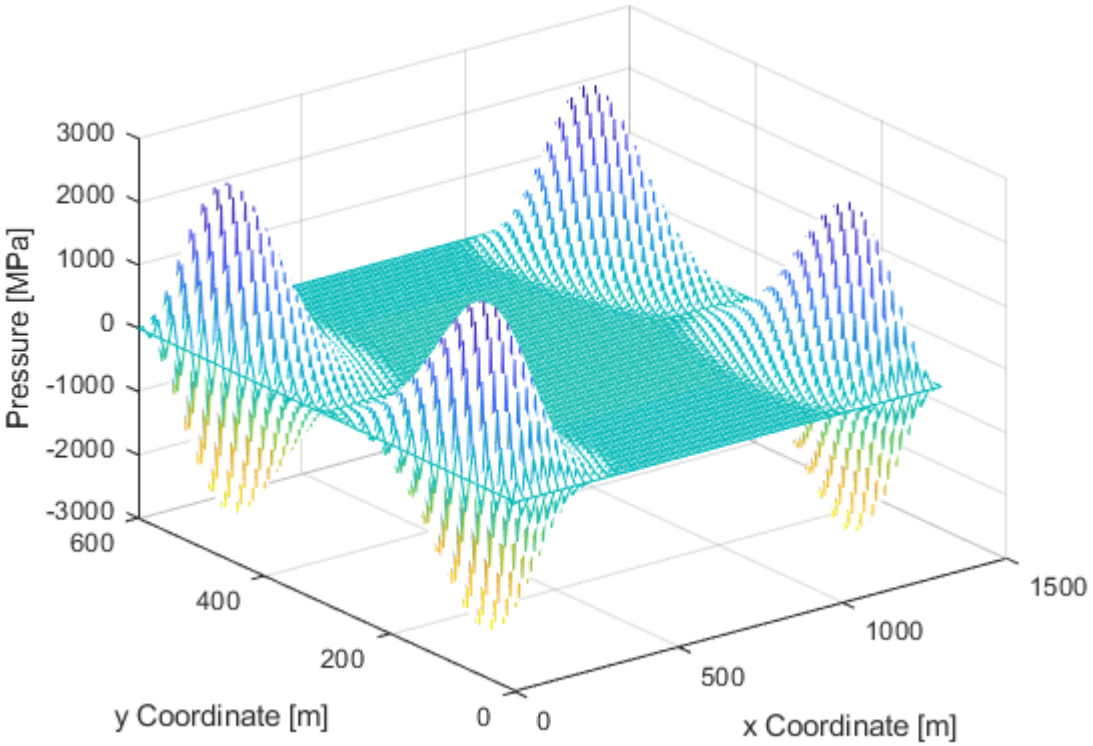


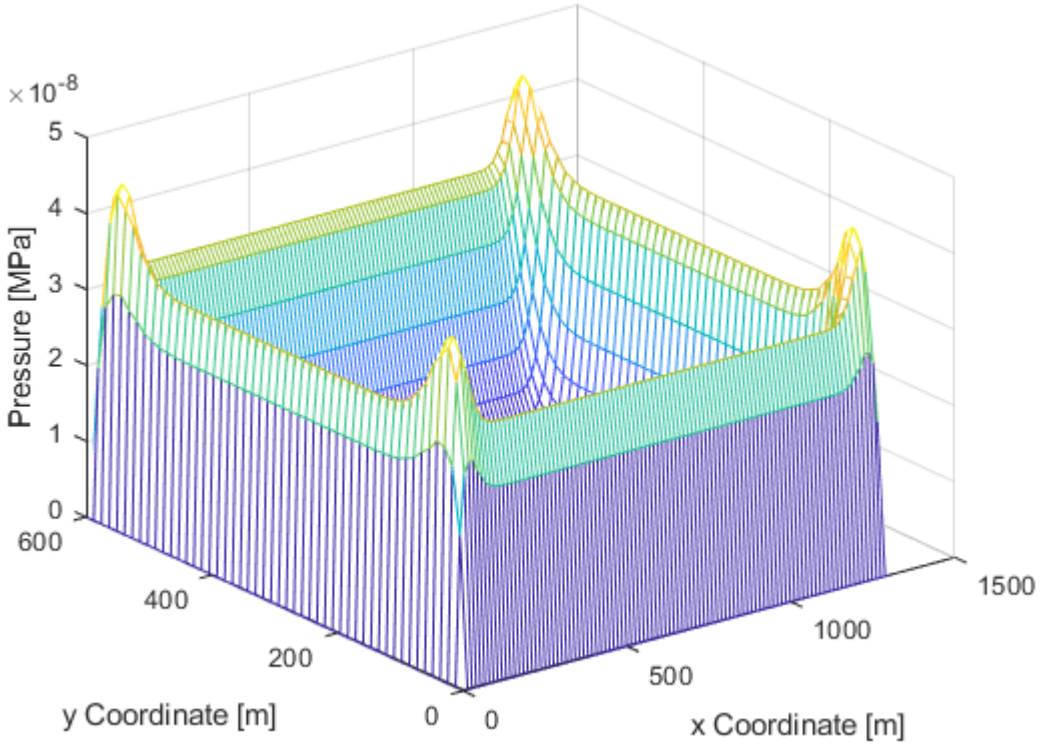

Pressure [MPa]
20
15
10
5
0
600
400
200
0
y Coordinate [m]
0
500
1000
1500
x Coordinate [m]

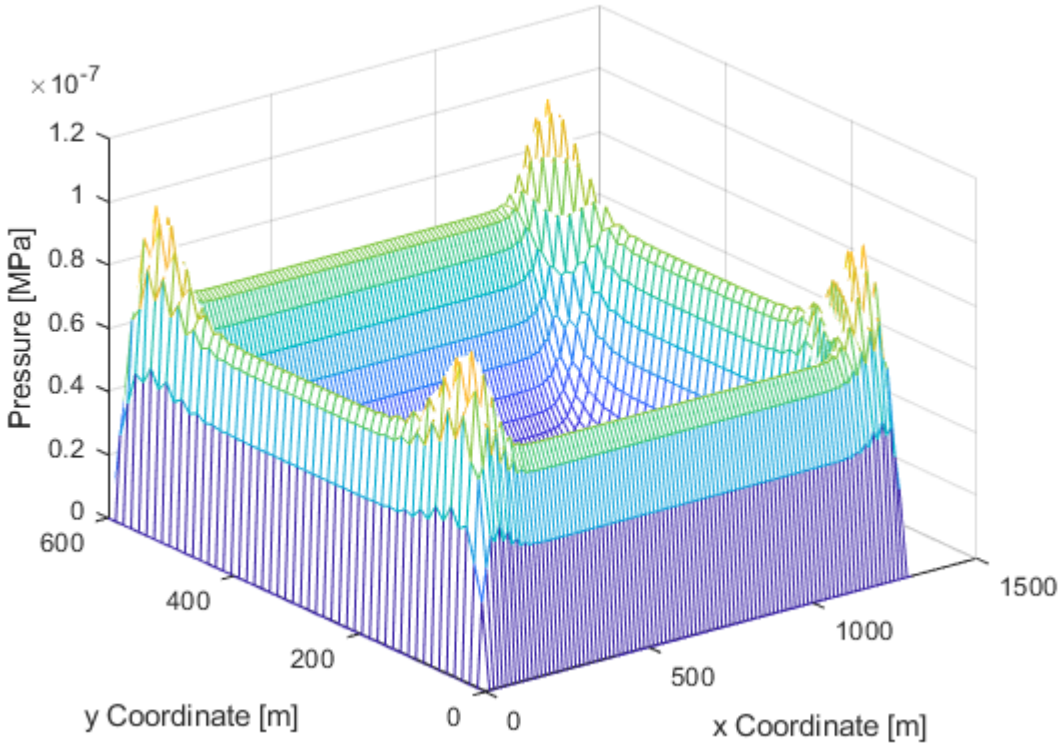

Pressure [MPa]
20
15
10
5
0
600
400
200
0
y Coordinate [m]
0
500
1000
1500
x Coordinate [m]

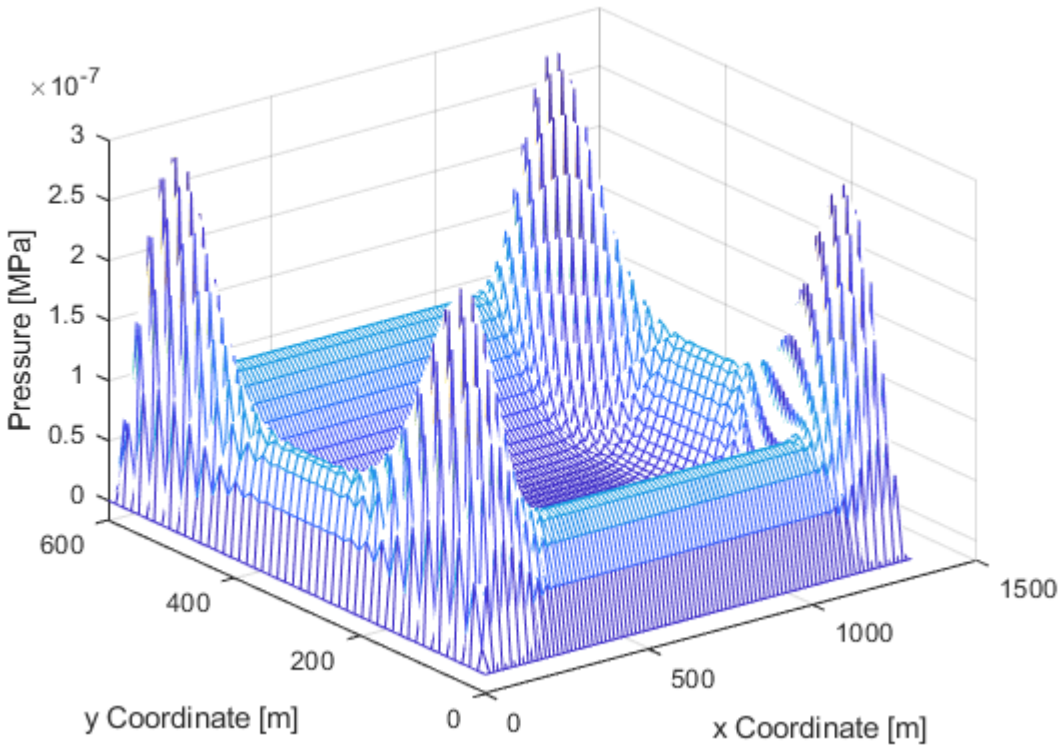

Pressure [MPa]
20
15
10
5
0
-5
600
400
200
0
y Coordinate [m]
0
500
1000
1500
x Coordinate [m]

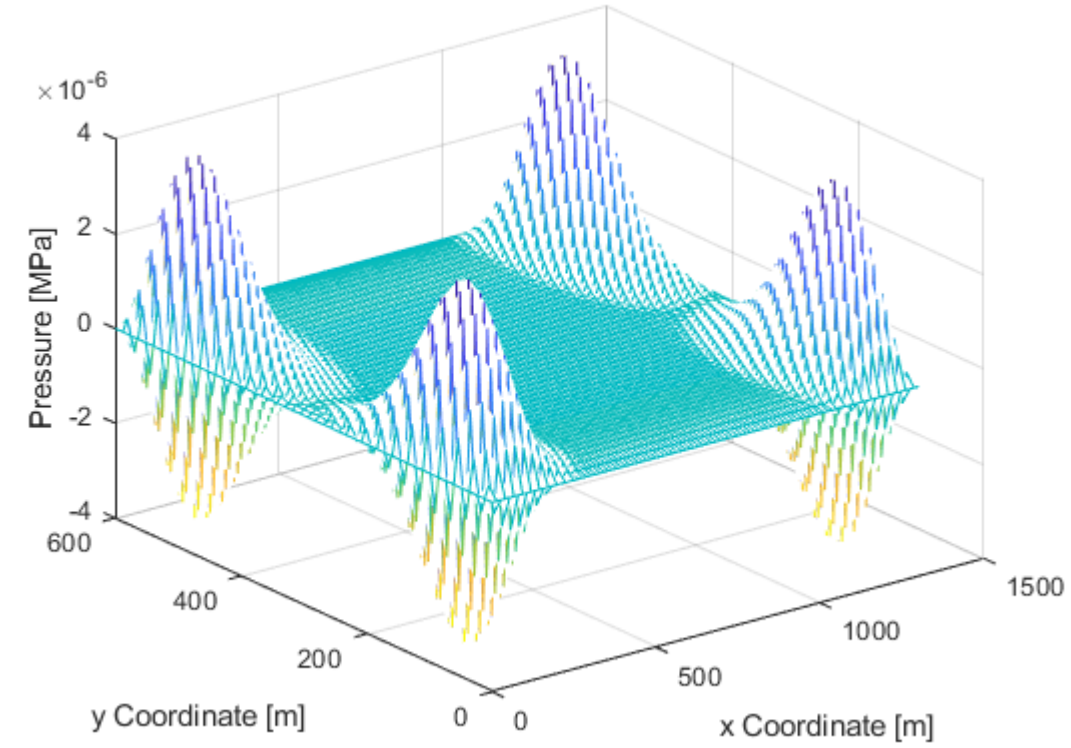

Pressure [MPa]
150
100
50
0
-50
-100
-150
600
400
200
0
y Coordinate [m]
0
500
1000
1500
x Coordinate [m]

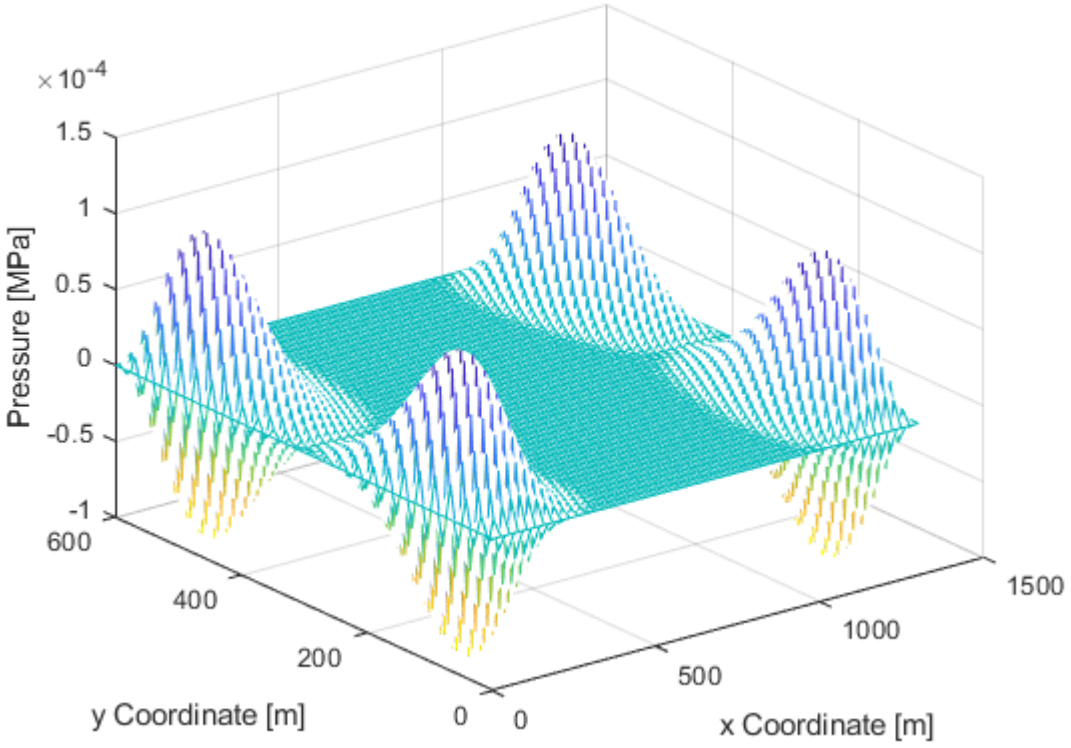

Pressure [MPa]
3000
2000
1000
0
-1000
-2000
-3000
600
400
200
0
y Coordinate [m]
0
500
1000
1500
x Coordinate [m]


×10^-8
5
4
3
2
1
0
Pressure [MPa]
600
400
200
0
y Coordinate [m]
0
500
1000
1500
x Coordinate [m]


×10^-7
1.2
1
0.8
0.6
0.4
0.2
0
Pressure [MPa]
600
400
200
0
y Coordinate [m]
0
500
1000
1500
x Coordinate [m]


×10^-7
3
2.5
2
1.5
1
0.5
0
Pressure [MPa]
600
400
200
0
y Coordinate [m]
0
500
1000
1500
x Coordinate [m]





Published with MATLAB® R2018a